



Flanders
State of
the Art

16_023_3
FHR reports

Manoeuvring Models

Sub report 3
KCS: 6 DOF manoeuvring model with full roll coupling

DEPARTMENT
MOBILITY &
PUBLIC
WORKS

www.flandershydraulicsresearch.be

Manoeuvring Models

Sub report 3 – KCS: 6 DOF manoeuvring model with full roll coupling

Delefortrie, G.; Eloit, K.; Vantorre, M.; Mostaert, F.

Legal notice

Flanders Hydraulics Research is of the opinion that the information and positions in this report are substantiated by the available data and knowledge at the time of writing.
 The positions taken in this report are those of Flanders Hydraulics Research and do not reflect necessarily the opinion of the Government of Flanders or any of its institutions.
 Flanders Hydraulics Research nor any person or company acting on behalf of Flanders Hydraulics Research is responsible for any loss or damage arising from the use of the information in this report.

Copyright and citation

© The Government of Flanders, Department of Mobility and Public Works, Flanders Hydraulics Research 2017
 D/2017/3241/277

This publication should be cited as follows:

Delefortrie, G.; Eloit, K.; Vantorre, M.; Mostaert, F. (2017). Manoeuvring Models: Sub report 3 – KCS: 6 DOF manoeuvring model with full roll coupling. Version 4.0. FHR Reports, 16_023_3. Flanders Hydraulics Research: Antwerp.

Until the date of release reproduction of and reference to this publication is prohibited except in case explicit and written permission is given by the customer or by Flanders Hydraulics Research. Acknowledging the source correctly is always mandatory.

Document identification


Customer:	Flanders Hydraulics Research	Ref.:	WL2017R16_023_3
Keywords (3-5):	KCS, manoeuvring, rolling		
Text (p.):	45	Appendices (p.):	/
Confidentiality:	<input checked="" type="checkbox"/> Yes	Released as from:	01/01/2025

Author(s):	Delefortrie, G.
------------	-----------------

Control

	Name	Signature
Reviser(s):	Eloit, K. Vantorre, M. (U-Gent)	
Project leader:	Delefortrie, G.	

Approval

Head of Division:	Mostaert, F.	
-------------------	--------------	--



Abstract

This report discusses the tests that have been carried out with the benchmark KCS ship model in the towing tank in the first half of 2017. An extensive open water manoeuvring program has been carried out, including the steering of the roll motion with the newly developed roll engine. The KCS is particularly affected by the roll motion due to its stern shape. This was also confirmed during a parametric roll test program. The 6 DOF manoeuvring model has been extended with additional terms to cope with the roll steering. The ship manoeuvring simulator has been accordingly adapted and fast time simulations have been carried out. These simulations revealed once more that additional tuning is needed to obtain a realistic manoeuvring behaviour.

fields of knowledge:

Manoeuvragedrag > Open water > Schaalmodelproeven

Manoeuvragedrag > Open water > Simulaties

Scheepsbeweging > Golfresponsie > Schaalmodelproeven

Contents

Abstract	III
Contents	V
List of tables.....	VII
List of figures	VIII
1 EXPERIMENTAL PROGRAM	1
1.1 Overview.....	1
1.2 Loading condition and under keel clearances	1
1.3 Open water test program	2
1.3.1 Overview.....	2
1.3.2 Implementation of the roll steering	4
1.4 Hydrostatic issues.....	7
1.4.1 Displacement.....	7
1.4.2 Roll dependency	7
1.5 Open water rudder lift and drag	7
1.5.1 Overview.....	7
1.5.2 Experimental observations.....	7
1.5.3 Comparison with CFD	9
1.6 Open water propeller thrust and torque.....	10
2 ROLL OBSERVATIONS.....	11
2.1 C0401.....	11
2.2 C0402.....	14
2.2.1 Free decay tests.....	14
2.2.2 Forced roll tests	15
2.3 Parametric rolling	16
2.3.1 Theory.....	16
2.3.2 Application for the KCS.....	17
2.3.3 Parametric roll model for the loading condition C0402.....	18
3 MATHEMATICAL MODEL	21
3.1 Improved set of equations	21
3.2 Model of propeller and rudder forces.....	21
3.3 Model of hull forces.....	22
3.3.1 Roll dependency	22

- 3.3.2 Other dependencies 27
- 3.4 Model of propulsion and steering induced forces 28
- 3.5 Validation..... 29
- 4 FAST TIME SIMULATIONS 30
 - 4.1 Changes to the source code 30
 - 4.1.1 Default values of tables and coefficients..... 30
 - 4.1.2 Fast time autopilot 30
 - 4.1.3 Full 4 DOF model 31
 - 4.1.4 Tuning of coefficients 32
 - 4.1.5 Functionality fixes..... 33
 - 4.1.6 Execution of test simulations 33
 - 4.2 Comparison with SIMMAN2014 results 34
 - 4.2.1 Captive tests 34
 - 4.2.2 Free running tests..... 35
 - 4.3 Standard manoeuvres: first iteration 37
 - 4.4 Standard manoeuvres: second iteration 39
 - 4.4.1 Acceleration trials..... 39
 - 4.4.2 Turning circles..... 41
 - 4.4.3 Zigzag tests 42
 - 4.4.4 Crash stop tests 43
- 5 CONCLUSIONS AND RECOMMENDATIONS 44
 - 5.1 Conclusions..... 44
 - 5.2 Recommendations..... 44
- 6 REFERENCES..... 45

List of tables

Table 1 – Ship’s main particulars	1
Table 2 – Forced harmonic roll parameters loading condition C0401	2
Table 3 – Forced harmonic roll parameters loading condition C0402 at zero speed	3
Table 4 – Forced harmonic roll parameters loading condition C0402 at 0.223, 0.449 and 0.589 m/s.....	3
Table 5 – Free roll decay tests in loading condition C0402	4
Table 6 – Parametric rolling: main wave parameters and their respective codes.....	17
Table 7 – Parametric rolling: ship forward speeds and their respective codes	18
Table 8 – Parametric rolling: waves and ship speed combination for head waves (HW) and following waves (FW)	18
Table 9 – Parametric rolling: test set up, parameters and codes.....	18
Table 10 – Comparison between measurements and mathematical model	29
Table 11 – Telegraph positions for the simulations	37

List of figures

Figure 1 – Lift and drag characteristic, original rudder, positive rotation direction: influence of speed	8
Figure 2 – Lift and drag characteristic, 0.5 m/s, positive rotation direction: influence of turbulence stimulation.....	8
Figure 3 – Measured lateral force on the rudder, 0.5 m/s, positive rotation direction: with (R1) and without (R3) turbulence stimulation.....	8
Figure 4 – Lift and drag characteristic: comparison between EFD and CFD.....	9
Figure 5 – Open water thrust coefficient	10
Figure 6 – Open water thrust and torque coefficient (all under keel clearances)	10
Figure 7 – Measured forces in 6 DOF during forced roll tests (series C0401A01).....	12
Figure 8 – Time series of roll moment during forced roll tests at zero speed (series C0401A01)	13
Figure 9 – Fourier analysis of the roll moment during forced roll tests at zero speed and high frequency (series C0401A01).....	13
Figure 10 – Transom emergence of the KCS with red water line at roll angles -5° , 0° and $+5^\circ$	13
Figure 11 – Pitch-roll coupling at high frequency.....	14
Figure 12 – Roll decay tests at 0.589 m/s.....	14
Figure 13 – Roll derivatives based on roll decay tests (series C0402G01)	15
Figure 14 – Roll derivatives based on forced roll tests (series C0402G01)	15
Figure 15 – Measured forces in 6 DOF during forced roll tests (series C0402G01)	16
Figure 16 – Full scale stability curves of the KCS at different loading conditions	17
Figure 17 – Example of parametric roll, test C0402G01_GEAX01: 0.223 m/s, head waves of 30 mm amplitude and $1.1 L_{pp}$ long	19
Figure 18 – Effect of A on the parametric rolling.....	19
Figure 19 – A as function of the pitch amplitude for following and head waves	20
Figure 20 – A : mathematical formulation for head waves.....	20
Figure 21 – Wake factors for the propeller thrust and shaft torque.....	21
Figure 22 – Wake factors for the rudder forces (no drift nor yaw).....	22
Figure 23 – Roll dependency model for the longitudinal force.....	23
Figure 24 – Roll angle dependent terms for the lateral force	23
Figure 25 – Roll velocity and acceleration dependency model for the lateral force	24
Figure 26 – Roll dependency model for the heave force	24
Figure 27 – Roll dependency model for the roll moment	25
Figure 28 – Roll dependency model for the pitch moment	25
Figure 29 – Roll dependency model for the yaw moment.....	26
Figure 30 – Drift functions for the loading condition C0401.....	27

Figure 31 – Propulsion dependency in the 1st quadrant 28

Figure 32 – Rudder dependency in the 1st quadrant..... 29

Figure 33 – Example of a 4 DOF COMPUTE table 30

Figure 34 – Example of a full tuning table 32

Figure 35 – COMPUTE simulation of the test C0401A01_MV0300: effect of the limit on the rudder induced yaw moment..... 33

Figure 36 – Comparison of resistance and propulsion tests between 2010 and 2017: 20% ukc, 0.62 m/s.... 34

Figure 37 – Comparison of rudder tests between 2010 and 2017: 20% ukc, 0.62 m/s 35

Figure 38 – Comparison between free running initial turning circles and different simulation alternatives. 35

Figure 39 – Comparison between free running zigzag tests and different simulation alternatives 36

Figure 40 – Obtained speeds (red curve indicates sinkage limit)..... 37

Figure 41 – First iteration turning circles..... 38

Figure 42 – First iteration zigzag trials..... 38

Figure 43 – Tuned manoeuvres 39

Figure 44 – Obtained speeds 39

Figure 45 – Selection of time series while acceleration at telegraph position Slow..... 40

Figure 46 – 35° turning circles at telegraph position Slow 41

Figure 47 – 20/20 zigzag tests at telegraph position Slow 42

Figure 48 – Crash stop test performance: evolution of propeller rate 43

Figure 49 – Crash stop tests starting from telegraph position Slow 43

1 EXPERIMENTAL PROGRAM

1.1 Overview

From January to June 2017 the KCS has been tested in the towing tank for different research projects:

- 00_009: execution of standard manoeuvres
- 12_034: manoeuvring in waves
- 17_001: SIMMAN 2019
- 17_025: CFD computations on rudders in open water

The current report will present the mathematical model of the tests executed in the frame of project 00_009, however information from 12_034 and 17_025 will also be used. Mind that for 17_001 no specific tests have been carried out, however, the speed conditions were chosen in accordance with SIMMAN 2014.

1.2 Loading condition and under keel clearances

Table 1 shows the most important main particulars of the KCS (ship C04). More information can be found in [1] and [2]. The largest \overline{GM} value was used to execute the tests in 00_009 and 12_034. With the intermediate \overline{GM} value forced roll tests, free decay tests and parametric roll tests have been carried out in 12_034. The smallest \overline{GM} value was applied during the tests executed in the frame of SIMMAN 2014.

Table 1 – Ship's main particulars

	Model scale	Full scale
L_{PP} [m]	4.367	230.0
B [m]	0.611	32.2
T [m]	0.2051	10.8
\overline{GM} [m]	0.0487 (C0401)	2.565
	0.0127 (C0402)	0.669
	0.011 (C01 – SIMMAN 2014)	0.6
I_{XX} [kgm ²]	13.9 (C0401)	-
	18.8 (C0402)	-
D_p [m]	0.150	7.9
A_R [m ²] Full	0.0196	54.45
	Movable part	40.78

The tests in 00_009 have been executed at 100% ukc, 50% ukc, 20% ukc and 10% ukc. The tests with C0402 were only executed at 100% ukc.

1.3 Open water test program

1.3.1 Overview

Table 2 – Forced harmonic roll parameters loading condition C0401

ukc	Speed [m/s]	φ_m [deg]	φ_a [deg]	T [s]	ukc	Speed [m/s]	φ_m [deg]	φ_a [deg]	T [s]
$\geq 50\%$	0	0	5	10	< 50%	0	0	2.5	5
		0	5	5			0	2.5	2.5
		0	4	2		0.248	0	2.5	5
	0	5	10	0			2.5	2.5	
	0.248	0	5	5		0.496	0	2.5	5
		0	4	2			0	2.5	2.5
		0	5	10		-0.142	0	2.5	5
	0	5	5	0			2.5	2.5	
	0.496	0	4	2		-0.354	0	2.5	5
		0	5	10			0	2.5	2.5
		0	5	5		0.851	0	5	10
	0	5	5	0			5	5	
	0	4	2	-0.142	0		5	10	
	0	5	5		0	5	5		
	0	4	2		-0.354	0	5	10	
	0	5	5	0		5	5		
	0	4	2	0		4	2		

Table 3 – Forced harmonic roll parameters loading condition C0402 at zero speed

φ_m [deg]	φ_a [deg]	T [s]	φ_m [deg]	φ_a [deg]	T [s]
0	6	6	0	5	2.9
0	9		0	5	2.5
0	6	4.8	0	2.5	2.15
0	9		0	2.5	1.91
0	6	4.5	0	2.5	1.72
0	9		0	2	1.58
0	6	4.2	0	2	1.45
0	9				
0	6				
0	9				
0	6	3.5			
0	9				

Table 4 – Forced harmonic roll parameters loading condition C0402 at 0.223, 0.449 and 0.589 m/s

φ_m [deg]	φ_a [deg]	T [s]	φ_m [deg]	φ_a [deg]	T [s]
0	6	6	0	6	4.2
0	9		0	9	
0	6	4.8	0	6	3.5
0	9		0	9	
0	6	4.5			
0	9				

During the tests the ship was always equipped with rudder and propeller. The common open water program executed for any ship with a single propeller and single rudder was extended with forced roll tests and tests at discrete heel angles different from zero. The speeds considered were (full scale values): -5 kn, -2 kn, 0 kn, 2 kn, 3.5 kn, 5 kn, 7 kn, 8.75 kn, 12 kn (only 50% ukc or more), 14 kn (only 50% ukc) and 17 kn (only 100 % ukc).

With the newly installed roll actuator, harmonic forced roll tests were carried out as follows:

$$\varphi(t) = \varphi_m + \varphi_a \sin\left(\frac{2\pi}{T}t\right) \quad (1)$$

The variations are different as a function of the under keel clearance and loading condition and are summarised in Table 2 for the loading condition C0401 and in Table 3 and Table 4 for the loading condition C0402.

In condition C0401 the heel of the ship was also slowly, harmonically varied from -5° to $+5^\circ$ (-2.5° to 2.5° for the smaller water depths) during the steady state condition when sailing at 0.142 m/s and for different drift angles. A selection of tests at zero drift angle was repeated at constant heel angles of $\pm 2.5^\circ$ and $\pm 5^\circ$, the latter only for under keel clearances $\geq 50\%$.

In condition C0402 free roll decay tests have been carried out according to Table 5.

Table 5 – Free roll decay tests in loading condition C0402

u [m/s]	φ_0 [deg]	u [m/s]	φ_0 [deg]	u [m/s]	φ_0 [deg]	u [m/s]	φ_0 [deg]
0	6	0.223	6	0.449	6	0.589	6
	9		9		9		9

1.3.2 Implementation of the roll steering

1.3.2.1 Execution of towing tank tests

Requirements

The roll actuator is steered as a MOTOR component from a PIOC. The MOTOR component is a new functionality, besides the analogue/digital input/output channels. In order to ensure a smooth steering the roll angle needs to be steered with 8 decimals and the acceleration has to be continuous all the time. On top of that the start and stop value of the heel angle has to be zero, because:

- The hydrostatic effect of the heel angle has to be excluded during the calibration time;
- Prior to some tests executions the MOTOR signal is HOMED with a fixed value, i.e. zero degrees.

At the beginning of the steady state interval the heel angle should be at its position according to equation (1). During the acceleration and deceleration the maximal heel angle needs to have a limited magnitude.

Acceleration

Similar formulae as for the acceleration of the other kinematic parameters during multi-modal tests can be used, however, the boundary conditions are different. The acceleration/deceleration time of the roll angle is never longer than the roll period itself⁽¹⁾, the boundary conditions are then:

- at $t = t_0 = 0$ (start roll acceleration):

$$f(t = t_0) = f_0 \equiv 0 \tag{2}$$

$$\dot{f}(t = t_0) = 0 \tag{3}$$

$$\ddot{f}(t = t_0) = 0 \tag{4}$$

¹ If the polynomial acceleration function would take longer than a roll period, the roll amplitude would reach too large values.

- at $t = t_r$ (end acceleration time, $T_{acceleration} = t_r$):

$$f(t = t_r) = f_r \quad (5)$$

$$\dot{f}(t = t_r) = \dot{f}_r \quad (6)$$

$$\ddot{f}(t = t_r) = \ddot{f}_r \quad (7)$$

In this case $f_0 \equiv 0$ the order of the polynomial acceleration function has to be larger compared to the one used in MULTI1 tests. The form of the acceleration function is:

$$f(t) = at^5 + bt^4 + ct^3 + dt^2 + et + f_0 \quad (8)$$

The initial conditions lead to:

$$d = 0 \quad (9)$$

$$e = 0 \quad (10)$$

$$f_0 \equiv 0 \quad (11)$$

while at the beginning of the steady state:

$$f(t = t_r) = at^5 + bt^4 + ct^3 = f_r \quad (12)$$

$$\dot{f}(t = t_r) = 5at^4 + 4bt^3 + 3ct^2 = \dot{f}_r \quad (13)$$

$$\ddot{f}(t = t_r) = 20at^3 + 12bt^2 + 6ct = \ddot{f}_r \quad (14)$$

Using Cramer's rule the determinant of the coefficient matrix is $-2t^9$. The values for a, b and c are then

$$a = \frac{-\ddot{f}_r t^6 + 6\dot{f}_r t^5 - 12f_r t^4}{-2t^9} = \frac{1}{2} \frac{\ddot{f}_r}{t^3} - 3 \frac{\dot{f}_r}{t^4} + 6 \frac{f_r}{t^5} \quad (15)$$

$$b = \frac{2\ddot{f}_r t^7 - 14\dot{f}_r t^6 + 30f_r t^5}{-2t^9} = -\frac{\ddot{f}_r}{t^2} + 7 \frac{\dot{f}_r}{t^3} - 15 \frac{f_r}{t^4} \quad (16)$$

$$c = \frac{-\ddot{f}_r t^8 + 8\dot{f}_r t^7 - 20f_r t^6}{-2t^9} = \frac{1}{2} \frac{\ddot{f}_r}{t_r} - 4 \frac{\dot{f}_r}{t_r^2} + 10 \frac{f_r}{t_r^3} \quad (17)$$

Deceleration

For the deceleration the methodology is analogous:

- at $t = t_s = 0$ (end of the steady state):

$$f(t = t_s) = f_s \quad (18)$$

$$\dot{f}(t = t_s) = \dot{f}_s \quad (19)$$

$$\ddot{f}(t = t_s) = \ddot{f}_s \quad (20)$$

- at $t = t_e$ (end of the roll deceleration, $T_{deceleration} = t_e$):

$$f(t = t_e) = 0 \quad (21)$$

$$\dot{f}(t = t_e) = 0 \quad (22)$$

$$\ddot{f}(t = t_e) = 0 \quad (23)$$

The form of the deceleration function is:

$$f(t) = at^5 + bt^4 + ct^3 + dt^2 + et + f \quad (24)$$

The initial conditions are:

$$d = 0.5\ddot{f}_s \quad (25)$$

$$e = \dot{f}_s \quad (26)$$

$$f = f_s \quad (27)$$

and at the end of the deceleration:

$$f(t = t_e) = at^5 + bt^4 + ct^3 + 0.5\ddot{f}_s t^2 + \dot{f}_s t + f_s = 0 \quad (28)$$

$$\dot{f}(t = t_e) = 5at^4 + 4bt^3 + 3ct^2 + \ddot{f}_s t + \dot{f}_s = 0 \quad (29)$$

$$\ddot{f}(t = t_e) = 20at^3 + 12bt^2 + 6ct + \ddot{f}_s = 0 \quad (30)$$

or

$$at^5 + bt^4 + ct^3 = -0.5\ddot{f}_s t^2 - \dot{f}_s t - f_s \quad (31)$$

$$5at^4 + 4bt^3 + 3ct^2 = -\ddot{f}_s t - \dot{f}_s \quad (32)$$

$$20at^3 + 12bt^2 + 6ct = -\ddot{f}_s \quad (33)$$

Using Cramer's rule the determinant of the coefficient matrix is again $-2t^9$. The values for a, b and c are then:

$$a = \frac{\ddot{f}_s t^6 + 6(-\dot{f}_s t - f_s)t^5 - 12(-0.5\ddot{f}_s t^2 - \dot{f}_s t - f_s)t^4}{-2t^9} = \frac{\ddot{f}_s t^6 + 6\dot{f}_s t^5 + 12f_s t^4}{-2t^9} = -\frac{1}{2} \frac{\ddot{f}_s}{t_e^3} - 3 \frac{\dot{f}_s}{t_e^4} - 6 \frac{f_s}{t_e^5} \quad (34)$$

$$b = \frac{-2\ddot{f}_s t^7 - 14(-\dot{f}_s t - f_s)t^6 + 30(-0.5\ddot{f}_s t^2 - \dot{f}_s t - f_s)t^5}{-2t^9} = \frac{-3\ddot{f}_s t^7 - 16\dot{f}_s t^6 - 30f_s t^5}{-2t^9} = \frac{3}{2} \frac{\ddot{f}_s}{t_e^2} + 8 \frac{\dot{f}_s}{t_e^3} + 15 \frac{f_s}{t_e^4} \quad (35)$$

$$c = \frac{\ddot{f}_s t^8 + 8(-\dot{f}_s t - f_s)t^7 - 20(-0.5\ddot{f}_s t^2 - \dot{f}_s t - f_s)t^6}{-2t^9} = \frac{3\ddot{f}_s t^8 + 12\dot{f}_s t^7 + 20f_s t^6}{-2t^9} = -\frac{3}{2} \frac{\ddot{f}_s}{t_e} - 6 \frac{\dot{f}_s}{t_e^2} - 10 \frac{f_s}{t_e^3} \quad (36)$$

1.3.2.2 Post processing

During the towing tank tests the heel angle of the ship is continuously monitored and the roll velocity is determined as follows $p = \frac{d\varphi}{dt} = \frac{\varphi_{i+1} - \varphi_i}{dt}$. This is analogous to the determination of the other kinematic parameters, but the position of the roll engine has more noise, which sometimes generates roll velocities different from zero when the heel angle is constant. In case of a constant heel angle the roll velocity is therefore by default equal to zero. This is also the case when no roll engine is present (for backwards compatibility). In case of harmonic roll motions, the roll velocity and acceleration are computed analytically.

The datapoint files used for regression analysis has been adapted as follows:

- Ship positions:
 - Xpos
 - Ypos
 - ROL: if a roll engine is present, its position (the heel angle) is written here. The default dimension is degrees. If the ship is free to roll, the registered position is also written in this column. In all other cases “-“ is written in the column.
 - Psipos
- Ship velocities
 - Su
 - Sv
 - Sp
 - Sr
- Ship accelerations
 - Sudot
 - Svdot
 - Spdot
 - Srdot

1.4 Hydrostatic issues

1.4.1 Displacement

During the experimental program some disagreements were found between the theoretical and actual hydrostatic behaviour of the vessel. According to SIMMAN and ORCA 3D the displacement of the ship model at the design draft is 356.2 kg, however after ballasting the measured displacement was 354.4 kg. At the same time the longitudinal position of the centre of gravity had an offset of 5 mm. The ship was ballasted several times during the course of the project. During the final ballast an increase of 1.7 mm was observed in the draft. After finishing the experimental program the weight of the empty ship was 155.5 kg, which is 2.5 kg more compared to the start of the experimental program and which can be ascribed to water absorption of the ship model during the tests.

1.4.2 Roll dependency

According to ORCA a 5° heel angle should generate a decrease of the average draft (-1.7 mm), however in practice an increase of the draft was observed (+0.3 mm). Moreover rolling to portside or to starboard side with the same angle resulted in a different average draft, which suggests a starboard – portside misalignment.

1.5 Open water rudder lift and drag

1.5.1 Overview

Open water tests with the movable part of the rudder have been carried out in the following conditions:

- Original rudder: series R1C04A01 (*none*);
- Rudder with turbulence stimulation strips at the leading edge (both in front and aft): R2C04A01 (*semi*);
- Rudder fully covered with turbulence stimulation strips: R3C04A01 (*full*).

A multi-modal test program, covering the 360° inflow, was carried out for each rudder at 0.5 and 1 m/s and in two rotation directions (+/-). Initially 1.5 m/s and 2.0 m/s were also planned, but these could not be carried out due to problems with the rudder torque gauge and the carriage.

1.5.2 Experimental observations

1.5.2.1 Effect of the speed

Figure 1 shows the speed influence on the original rudder. A larger speed will induce a somewhat maximal larger lift, but especially in the astern condition, which is larger than the ahead condition. At the same time some phase shift is observed in the drag. Contrary to what could be expected, the results seem better at 0.5 m/s. At this lower speed the curves show more symmetry and the maximal drag is smaller. The latter is important for the comparison with CFD, see 1.5.3.

Figure 1 – Lift and drag characteristic, original rudder, positive rotation direction: influence of speed

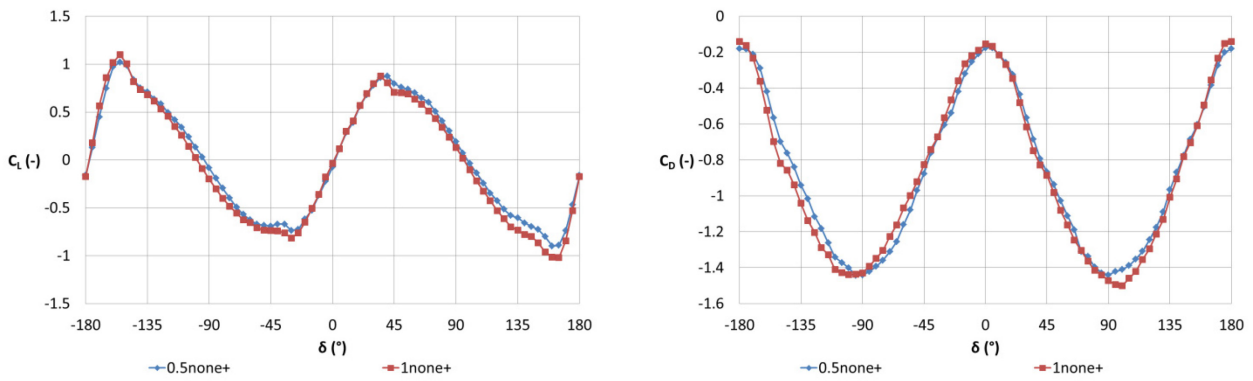


Figure 2 – Lift and drag characteristic, 0.5 m/s, positive rotation direction: influence of turbulence stimulation

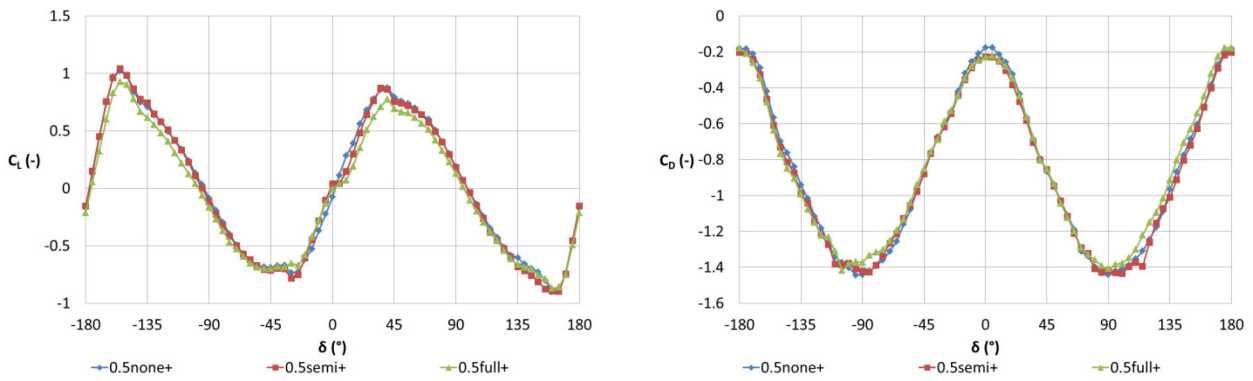
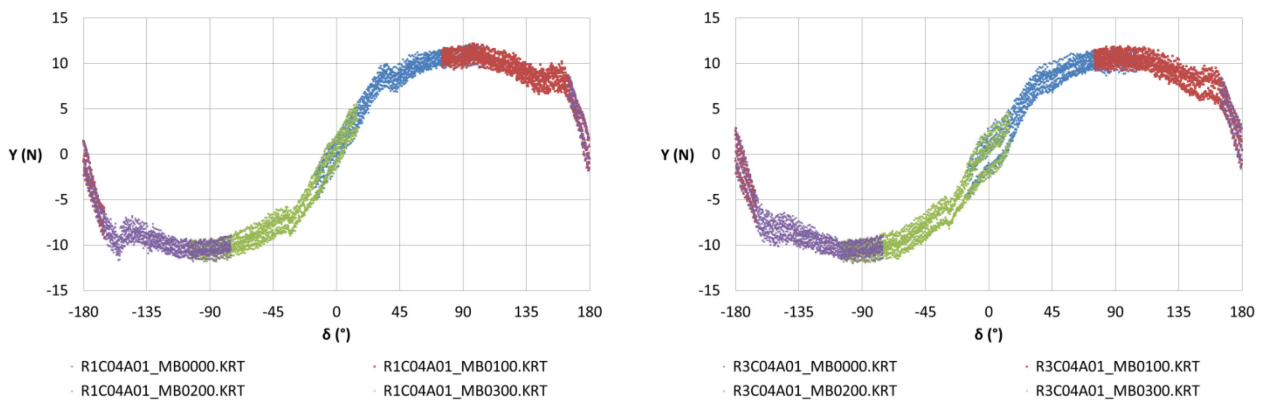


Figure 3 – Measured lateral force on the rudder, 0.5 m/s, positive rotation direction: with (R1) and without (R3) turbulence stimulation



1.5.2.2 Effect of the turbulence stimulation

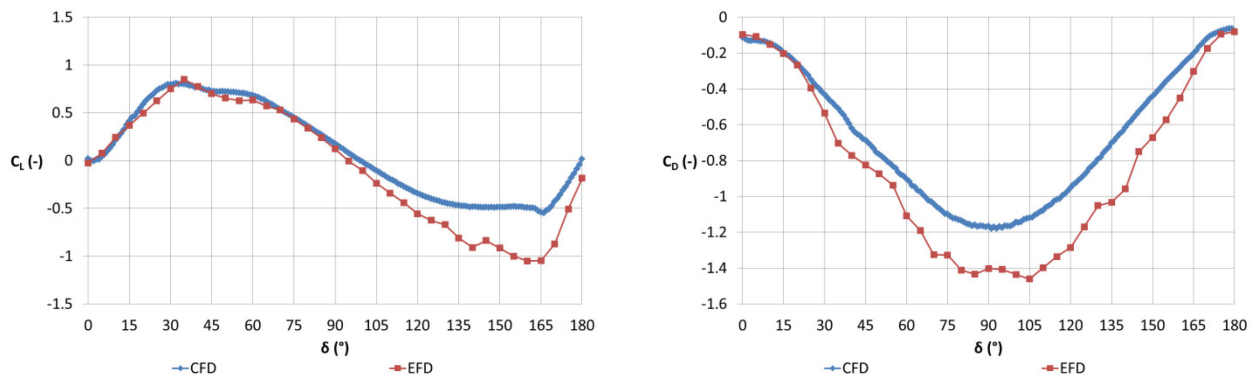
The lift and drag characteristic of the different rudders is plotted in Figure 2. A gentle turbulence stimulation has some minor effects compared to the original rudder. The most pronounced effect is the decreasing of the lift for small inflow angles, which is even more the case if the rudder is fully covered with turbulence stimulation material. At the same time the drag is increased and is in general less symmetric when turbulence stimulation is applied.

The smaller lift for small inflow angles is due to an oscillatory behaviour of the lateral force when turbulence stimulation is applied, see Figure 3. In general the original rudder seems to generate the best drag and lift characteristic.

1.5.3 Comparison with CFD

Figure 4 shows the comparison between the selected open water characteristic from the towing tank tests and the CFD computation. Both agree very well for inflow angles up to 20°. From there on the increase of lift will be somewhat larger in CFD, but both EFD and CFD attain similar values for the maximal lift as stall occurs earlier in CFD. The drag in EFD is larger compared to CFD as is the lift for reversed inflow angles.

Figure 4 – Lift and drag characteristic: comparison between EFD and CFD



1.6 Open water propeller thrust and torque

The open water data of the propeller are available on the SIMMAN website, however, only for the first quadrant. To obtain the data in 4 quadrants the most resembling Wageningen B series was selected, which is the B5-75 at a P/D ratio of 1. The curves of the B5-75 propeller were adapted to match the SVA data near the first quadrant, see Figure 5. The resulting curves for the KCS have been plotted in Figure 6.

Figure 5 – Open water thrust coefficient

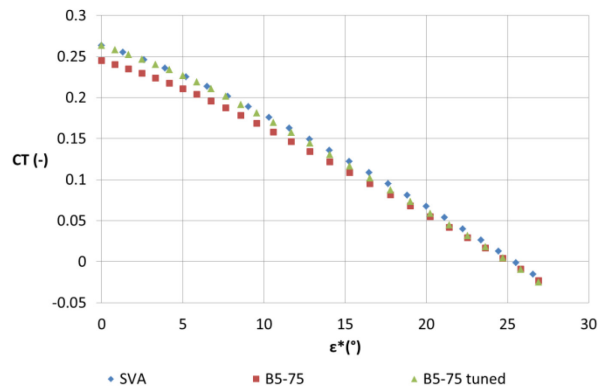
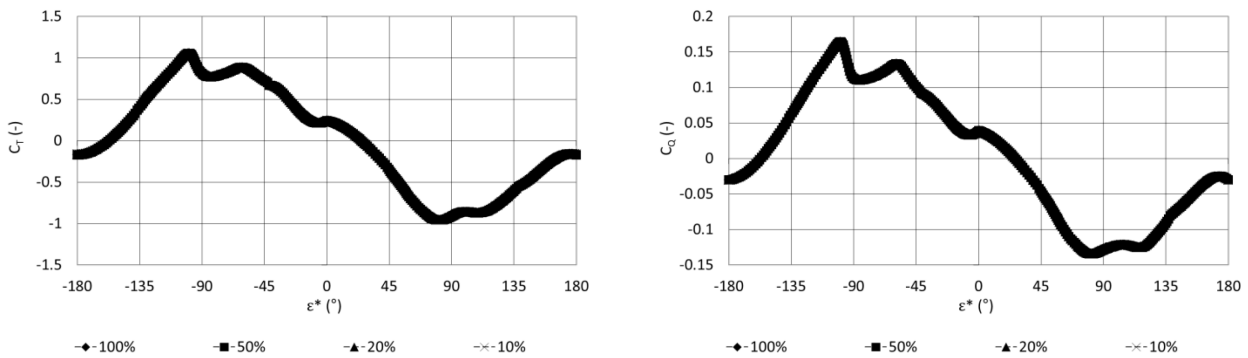


Figure 6 – Open water thrust and torque coefficient (all under keel clearances)



2 ROLL OBSERVATIONS

2.1 C0401

In this loading condition only forced roll tests have been carried out. In this paragraph the most remarkable findings will be discussed using the following definitions:

- low frequency roll: 5° amplitude, 10 s period;
- high frequency roll: 4° amplitude, 2 s period.

To have an idea of the effect of forced roll motion on the forces and moments some results have been plotted as a function of the roll angle in Figure 7:

- the effect of the roll angle on the longitudinal force seems marginal;
- the same is the case for the yaw moment, unless a high frequency motion is applied;
- this high frequency motion was introduced in the program, because originally only low frequency motions were applied, however, such low frequency motion only generates a hydrostatic effect for the roll moment and higher frequencies are needed to detect the dependency of the roll acceleration and velocity;
- these hydrostatic effects are not only visible on the roll moment, but also on the lateral force, heave force and pitch moment⁽²⁾. For the heave the hydrostatic effect is opposite to what was expected (see 1.4.2) and a quadratic relationship with the roll angle is observed. The same is true for the pitch moment, however, higher order effects are observed at larger frequencies;
- In case of the sway force, a significant share of the effect should be ascribed to the connection between the roll torque gauge and lateral force gauge. During ship calibration 20 Nm roll torque induced -5N sway force.

To have more insight in the influence of the frequency the time series for the roll moment during the forced roll tests at zero speed have been plotted in Figure 8. At low frequency the signal is regular and can be described by a first order harmonic, however at high frequency the signal seems more scattered. At first thought this could be ascribed by the formation of a wave system due to the high frequency, however, Fourier analysis in Figure 9 reveals that the signal is periodic with a strong fifth order harmonic and that the measurement is thus repeatable. The same effect is observed for the pitch moment which indicates a pitch-roll coupling.

Figure 10 shows a view of the transom of the KCS at different heeled water lines. While rolling a large part of the transom emerges from the water. At high frequency the pitch response to the roll movement is delayed due to the increased damping⁽³⁾, see Figure 11:

- The test starts at almost zero trim with a movement towards positive roll angles;
- The trim responds hydrostatically with a negative angle, however with some delay;
- The recovery of the trim is slower compared to the recovery of the roll towards zero degrees and shows even overshoot.

The fifth order component is then ascribed to:

- The hydrostatic component (base);
- The combinations of roll (velocity, acceleration) and pitch (roll+ pitch+, roll + pitch-, roll- pitch+, roll- pitch-).

² During the tests the ship is free to heave and pitch. A corresponding hydrostatic heave force and pitch moment is computed [5].

³ The reviewers questioned whether damping or inertia is to be taken responsible. According to section 2.2.2 (although with a different loading condition) an increased damping is noted with increasing frequency.

Figure 7 – Measured forces in 6 DOF during forced roll tests (series C0401A01)

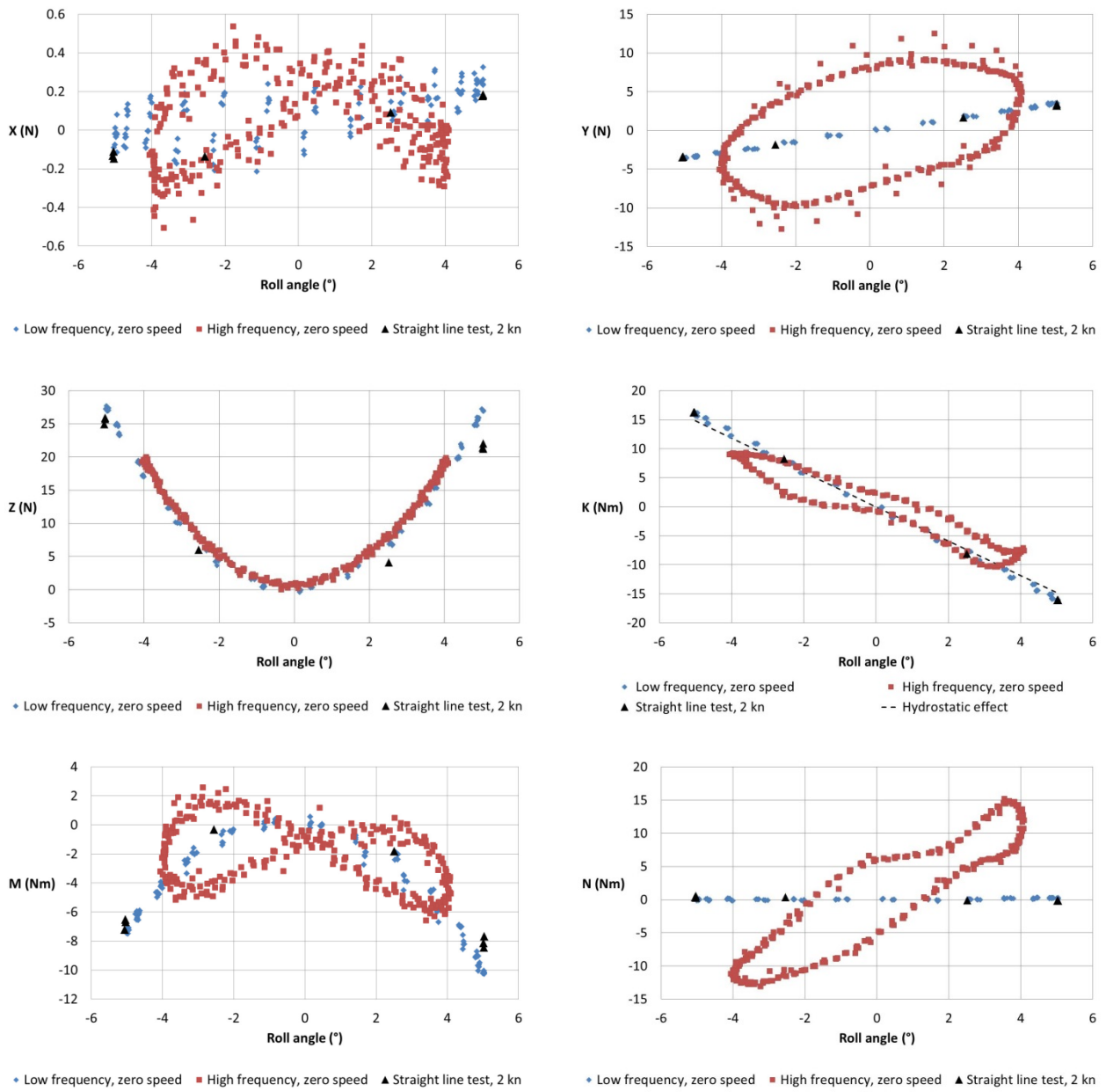


Figure 8 – Time series of roll moment during forced roll tests at zero speed (series C0401A01)

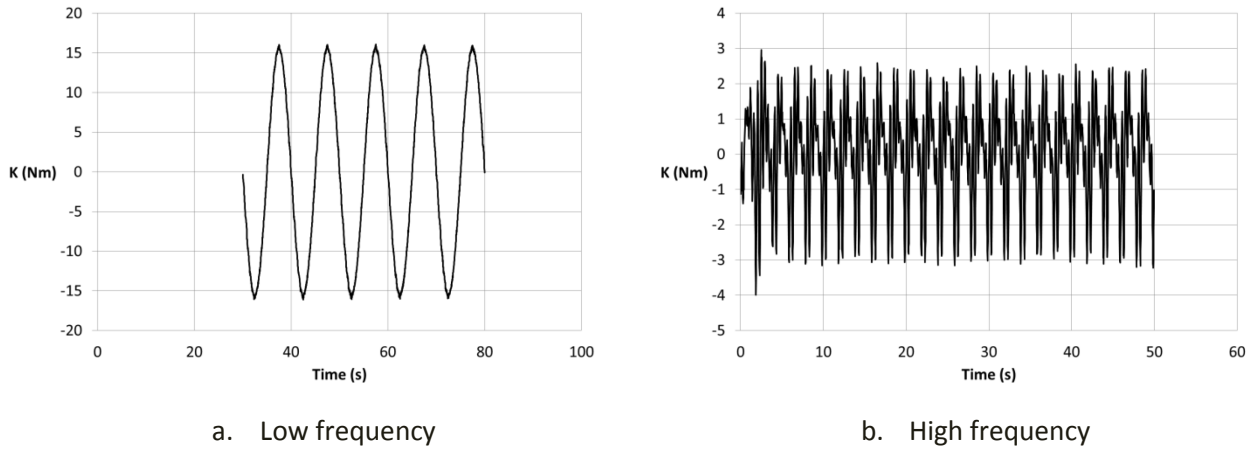


Figure 9 – Fourier analysis of the roll moment during forced roll tests at zero speed and high frequency (series C0401A01)

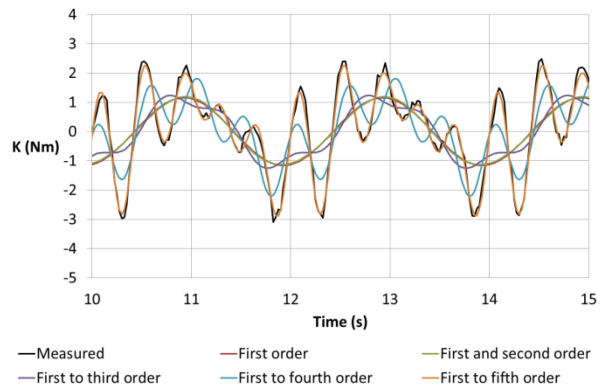


Figure 10 – Transom emergence of the KCS with red water line at roll angles -5° , 0° and $+5^\circ$

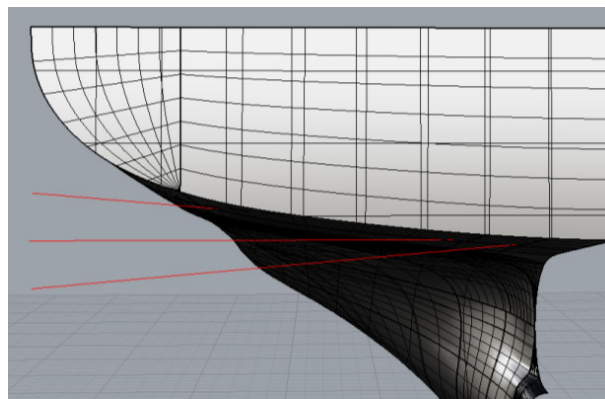
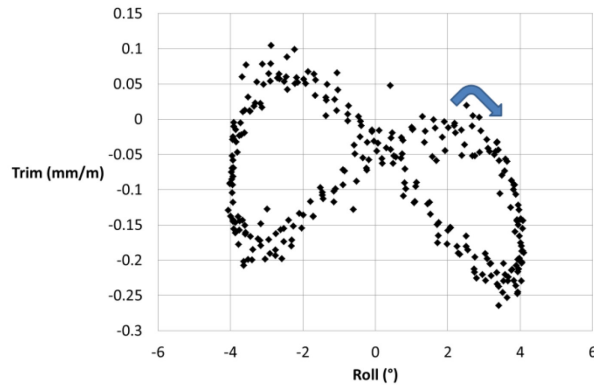


Figure 11 – Pitch-roll coupling at high frequency



2.2 C0402

In this loading condition both roll decay tests and forced roll tests have been carried out.

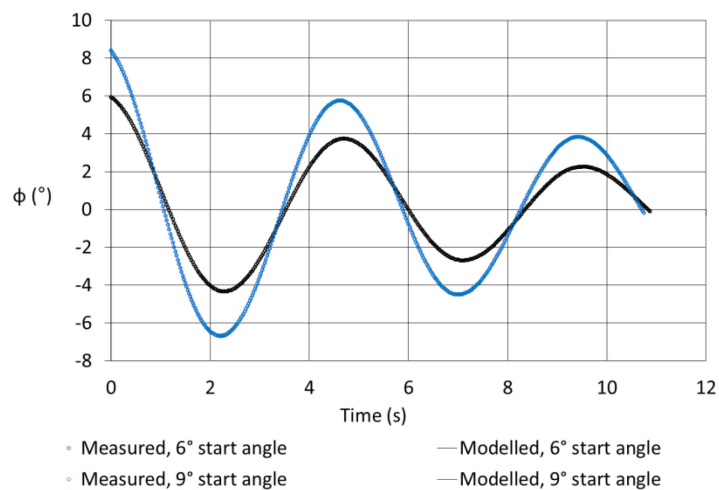
2.2.1 Free decay tests

Roll decay tests have been carried out at four different forward speeds (0, 0.223, 0.449 and 0.589 m/s) and at two initial angles (6 and 9°). An example of the decay motion can be found in Figure 12. The fit on the figure is a linear, first order fit:

$$(K_{\dot{p}} - I_{xx})\dot{p} + K_p p - mg\overline{GM}\varphi = 0 \quad (37)$$

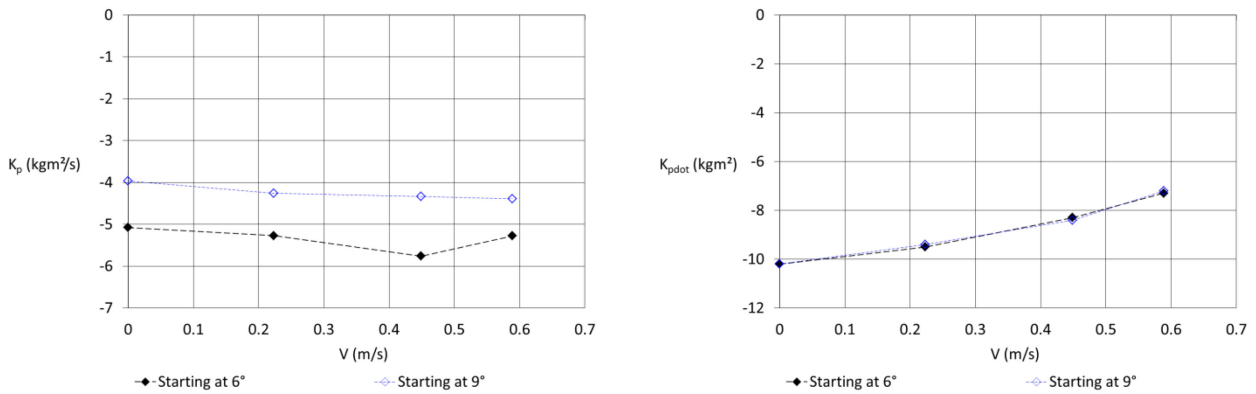
Both model and measurement coincide in Figure 12.

Figure 12 – Roll decay tests at 0.589 m/s



The roll period varies between 4.8 s and 5.1 s, respectively for the fastest and slowest tests. This means that both $K_{\dot{p}}$ and K_p are speed dependent. Moreover the decay is weaker when the initial angle is larger, in other words K_p is smaller for the tests starting at 9°, see also Figure 13.

Figure 13 – Roll derivatives based on roll decay tests (series C0402G01)



2.2.2 Forced roll tests

In the first place the results from the forced roll tests are compared with the results from the free decay tests by fitting the measured roll moment with equation (37). The effect of sailing speed and roll amplitude are confirmed and the predicted roll derivatives are of the same magnitude as for the roll decay tests, see Figure 14. Based on the forced roll tests, the influence of the roll frequency can be analysed as well. The roll added moment decreases with increasing frequency to reach a minimal value at a certain speed dependent frequency. With increasing frequency the roll added moment starts to increase again. The roll damping derivative increases more or less linearly with the roll frequency.

Figure 14 – Roll derivatives based on forced roll tests (series C0402G01)

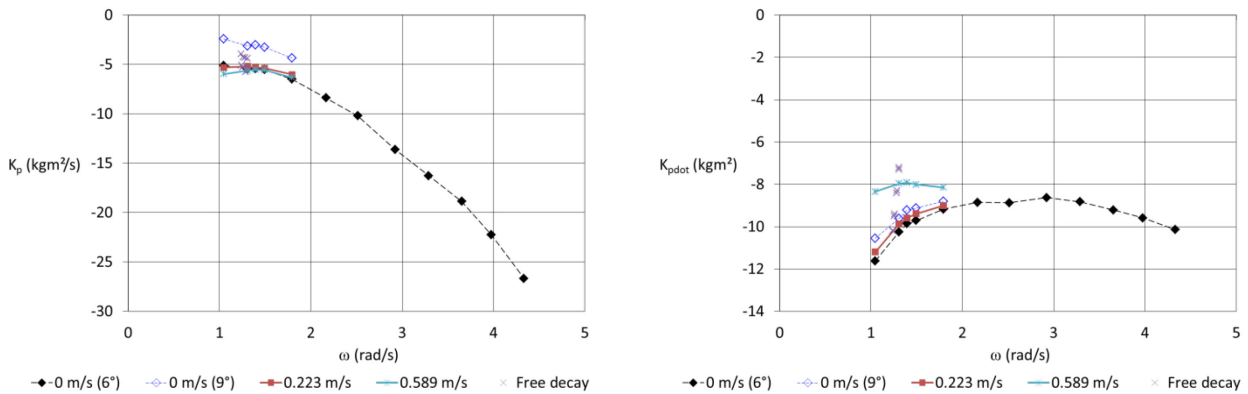
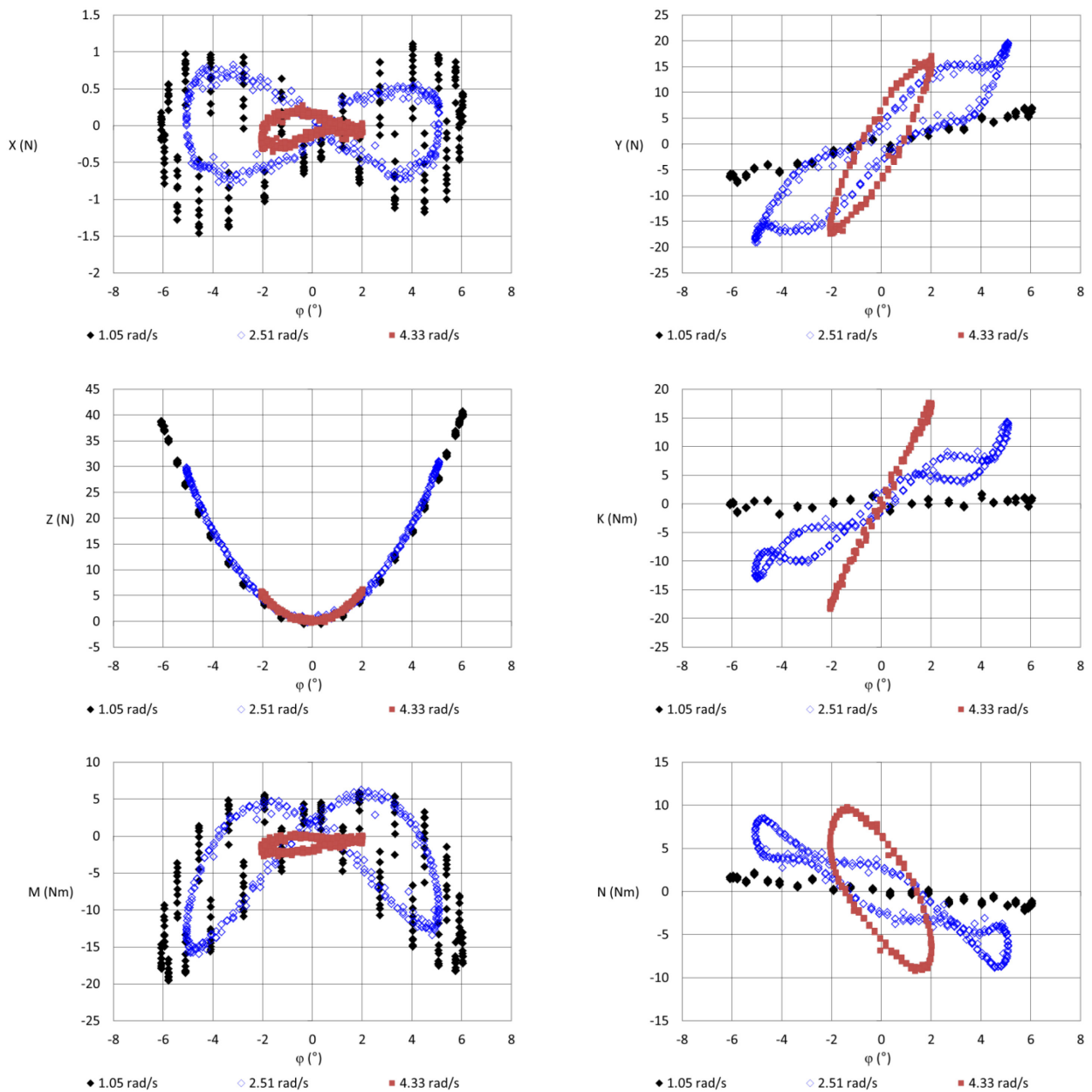


Figure 15 shows the measured forces and moments in 6 DOF for a set of roll frequencies:

- For the longitudinal and heave force, the same conclusions can be drawn as in loading condition C0401;
- Both the yaw moment and the sway force seem significantly influenced by the roll frequency. The effect of the roll frequency has an opposite sign compared to the loading condition C0401;
- The same is true for the roll moment, which has to be ascribed to the increased effect of the roll (added) moment of inertia and the decreased hydrostatic effect (due to the smaller \overline{GM}) compared to the loading condition C0401;
- As for the loading C0401, a strong connection can be observed between pitch and roll. However, at very high roll frequencies, the pitch seems to remain constant and cannot longer follow the roll motion.

Figure 15 – Measured forces in 6 DOF during forced roll tests (series C0402G01)



2.3 Parametric rolling

2.3.1 Theory

The phenomenon of parametric rolling resonance is ascribed due to an instability inception caused by \overline{GM} variations due to wave action. The roll equation, with a time dependent \overline{GM} can be written as:

$$(K_{\dot{p}} - I_{xx})\dot{p} + K_p p - mg\overline{GM}(t)\varphi = 0 \quad (38)$$

Due to first order wave action with wave encounter frequency ω_e , $\overline{GM}(t)$ can be estimated as:

$$\overline{GM}(t) = \overline{GM}_0 + \overline{GM}_W \sin \omega_e t \quad (39)$$

And the roll equation can be rewritten as:

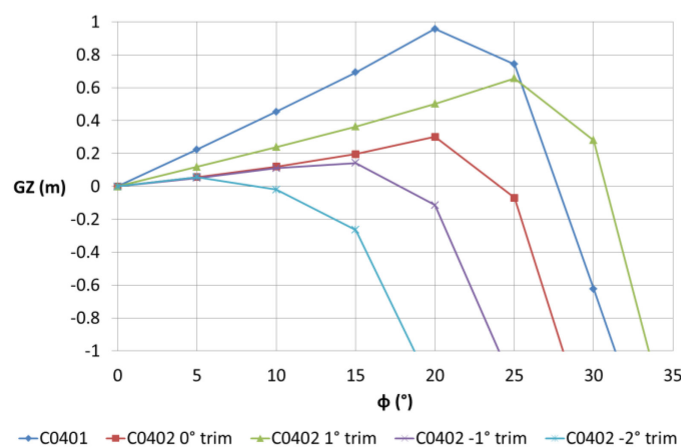
$$(K_{\dot{p}} - I_{xx})\dot{p} + K_p p - mg[\overline{GM}_0 + \overline{GM}_W \sin \omega_e t]\varphi = 0 \quad (40)$$

If the damping is neglected the above equation is a so-called Mathieu equation. For certain frequencies ω_e the solution of the equation becomes infinite, which is the case when the wave encounter frequency equals 0.5 times the natural roll frequency. See [4] for more information.

2.3.2 Application for the KCS

The effect of the wave profile on the stability curves has not yet been computed, but as an alternative Figure 16 shows the stability curves at different loading conditions, among trimmed conditions. It is clear that for condition C0402 a bow down trim will quickly result in unstable behaviour due to the rise of the stern section of the ship. Parametric rolling is thus likely to occur whenever the stern emerges due to wave induced pitch action.

Figure 16 – Full scale stability curves of the KCS at different loading conditions



42 tests have been carried out as follows:

- 8 wave frequencies and 3 wave amplitudes have been selected according to Table 6;
- 8 ship’s velocities according to Table 7;
- Ship velocity and wave climate have been combined so that the encounter frequency was around 2.24 s or 50% of the numerically computed natural roll period. Please observe that this numerical period, 4.48 s is slightly below the experimental period, which was yet unknown when executing the parametric roll tests. The different combinations are shown in Table 8 and Table 9.

If parametric roll occurred, in 31 of the 42 tests, the test was aborted once the roll angle reached 6° to avoid capsizing of the ship model. Three tests, namely the zero speed tests in wave codes U, V, W did not produce any useful results and will be disregarded, thus parametric roll occurred in 80% of the tests.

Table 6 – Parametric rolling: main wave parameters and their respective codes

code	lw/Lpp	T (s)	ζ_a1 (mm)	Code	ζ_a2 (mm)	Code	ζ_a3 (mm)	Code
w1	0.60	1.49	15	A	20	I	30	Q
w2	0.70	1.69	15	B	20	J	30	R
w3	0.80	1.89	15	C	20	K	30	S
w4	0.90	2.09	15	D	20	L	30	T
w5	0.97	2.24	15	E	20	M	30	U
w6	1.00	2.30	15	F	20	N	30	V
w7	1.02	2.34	15	G	20	O	30	W
w8	1.10	2.50	15	H	20	P	30	X

Table 7 – Parametric rolling: ship forward speeds and their respective codes

code	VFS (knots)	VMS (m/s)	Code
v1	0.0	0.000	A
v2	0.6	0.045	B
v3	1.1	0.081	C
v4	1.8	0.128	D
v5	3.2	0.223	E
v6	4.1	0.293	F
v7	6.3	0.449	G
v8	8.3	0.589	H

Table 8 – Parametric rolling: waves and ship speed combination for head waves (HW) and following waves (FW)

	HW			FW
v1	w6	w5	w7	---
v2	w5	w6	w7	---
v3	w5	w7	w6	---
v4	---	---	---	w4
v5	---	w8	---	---
v6	---	---	---	w3
v7	---	---	---	w2
v8	---	---	---	w1

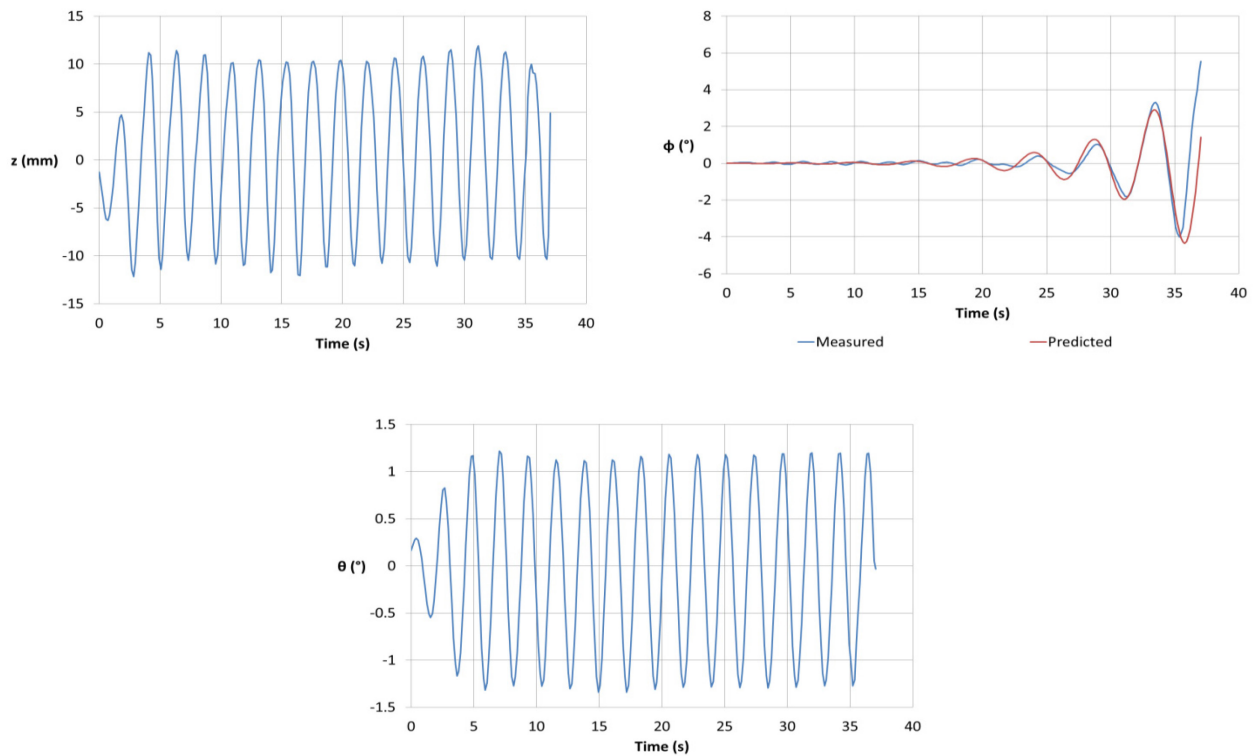
Table 9 – Parametric rolling: test set up, parameters and codes

test	Codes				
	V	Wave			sign(u)
1	A	E	M	U	+
2	A	F	N	V	+
3	A	G	O	W	+
4	B	E	M	U	+
5	B	F	N	V	+
6	B	G	O	W	+
7	C	E	M	U	+
8	C	F	N	V	+
9	C	G	O	W	+
10	D	D	L	T	-
11	E	H	P	X	+
12	F	C	K	S	-
13	G	B	J	R	-
14	H	A	I	Q	-

2.3.3 Parametric roll model for the loading condition C0402

The test results were post-processed as follows to allow a more in depth study:

- A DPT-file was generated based on the KRT-files;
- The times were set at zero when the ship meets the first wave;
- Within this time frame the heave and pitch amplitude was modelled;
- If parametric rolling occurred a mathematical model was fitted.

Figure 17 – Example of parametric roll, test C0402G01_GEAX01: 0.223 m/s, head waves of 30 mm amplitude and 1.1 L_{PP} long


An example is shown in Figure 17. If parametric roll occurs the roll angle has more or less the following formulation:

$$\varphi(t) = Ae^{\mu t} \sin(\omega_{\varphi} t + \tau) \quad (41)$$

The roll angle seems to oscillate with the natural roll frequency ω_{φ} , which is related to the loading condition. Due to parametric rolling the amplitude increases exponentially with exponent μ . This exponent is also more or less the same for all tests. With each period the amplitude of the roll motion is multiplied with a factor 2.2, or for the present loading condition:

$$\mu = \omega_{\varphi} \frac{\ln 2.2}{2\pi} \approx 0.17 \quad (42)$$

The amplitude A indicates then how quickly the parametric roll starts after the ship encounters the wave. For example in Figure 17 $A \approx 0.01^{\circ}$. A has been computed for all tests and indicates then the parametric roll intensity. Figure 18 gives an idea on the effect of A on the roll angle evolution. This parametric roll intensity is strongly related to the modelled pitch amplitude, which for following waves is intensely connected to the wave profile:

$$\frac{\theta_A L_{PP}}{\zeta_A} = 0.18 \pm 0.02 \frac{^{\circ}m}{mm} \quad (43)$$

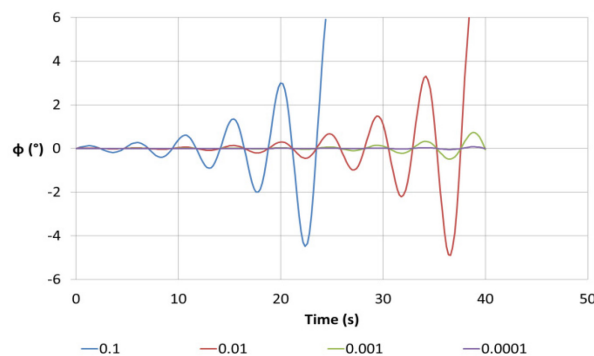
 Figure 18 – Effect of A on the parametric rolling


Figure 19 – A as function of the pitch amplitude for following and head waves

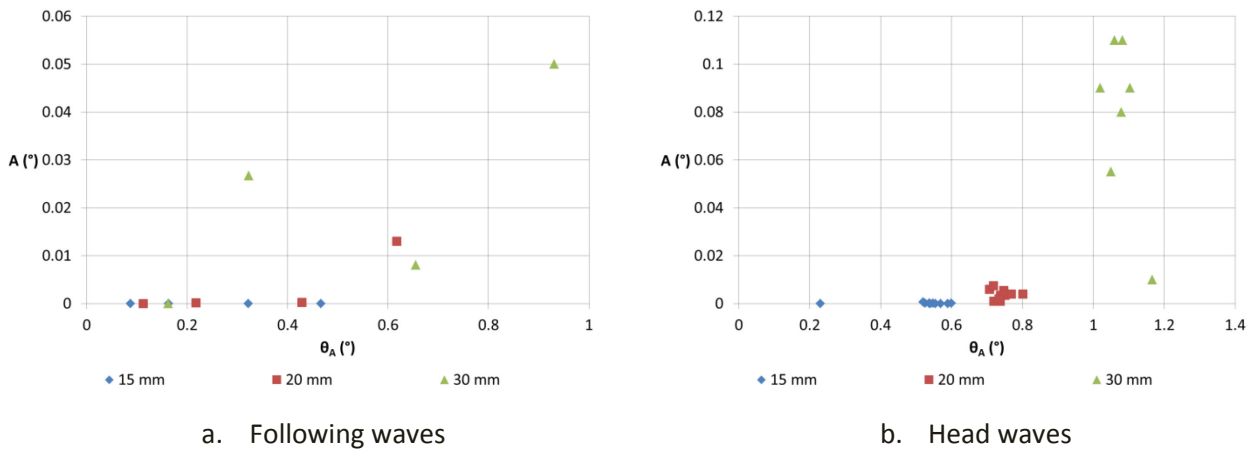


Figure 20 – A : mathematical formulation for head waves

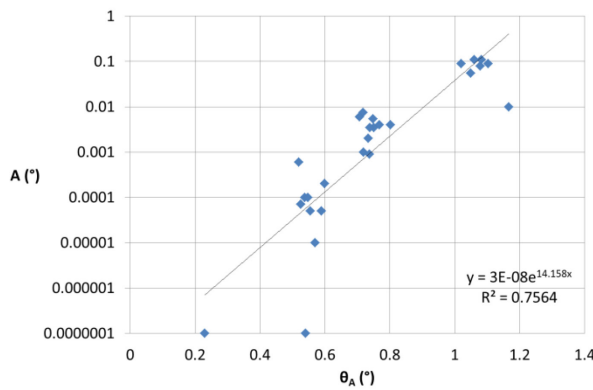


Figure 19 shows the resulting A -values for the different wave climates for all successfully executed tests. Parametric roll can be called significant once $A \geq 0.001^\circ$, which is the case if the ship starts to pitch with amplitude 0.7° in head waves and 0.5° in following waves (mind that there is one exception here). In all cases a wave amplitude of 15 mm was not enough to induce significant parametric rolling, however towards the end of such tests an onset towards parametric rolling can be observed. Apart from the link with the trim angle or wave profile the results seem scattered, which indicates the instability of the physical process. Some repeat tests would have been useful to check the repeatability of the phenomenon. Figure 20 shows an example for a mathematical model formulation of A as a function of the pitch amplitude.

This research should be continued with the analysis of the effect of the wave profile on the ship’s stability.

3 MATHEMATICAL MODEL

3.1 Improved set of equations

The effect of the static heel angle was already studied in [3], however at that time the heel angle was induced by changing the loading condition of the ship. At present the heel is imposed externally and the loading condition of the ship does not change. To cope with the effect of the captive roll motion the set of equations of motions has to be extended with the following green terms (already included in Regstatx, version 4.0 and above):

$$X_{IC} = m[-\dot{u} + vr + x_G r^2 + y_G \dot{r} - z_G pr] \quad (44)$$

$$Y_{IC} = m[-\dot{v} - ur - x_G \dot{r} + y_G r^2 + z_G \dot{p}] \quad (45)$$

$$Z_{IC} = 0 + m[vp - x_G pr - y_G \dot{p} + z_G p^2] \quad (46)$$

$$K_{IC} = -I_{xx} \dot{p} + I_{xz} \dot{r} - I_{yx} pr - I_{yz} r^2 + m[-vpy_G + (\dot{v} + ur)z_G] \quad (47)$$

$$M_{IC} = I_{xy} \dot{p} + I_{yz} \dot{r} - I_{xz}(p^2 - r^2) - (I_{xx} - I_{zz})pr + m[vpx_G + (-\dot{u} + vr)z_G] \quad (48)$$

$$N_{IC} = -I_{zz} \dot{r} + I_{xz} \dot{p} + I_{xy} p^2 + I_{yz} pr + m[-(\dot{v} + ur)x_G + (\dot{u} - vr)y_G] \quad (49)$$

The grey terms are still being neglected. A maximal heel angle of 5° means that the ship bound axis system rotates with 5° around the X axis of the horizontal bound system. A lateral variable is then influenced as follows, for instance the sway velocity of the homed ship is, when only the lateral carriage moves at velocity Y_v :

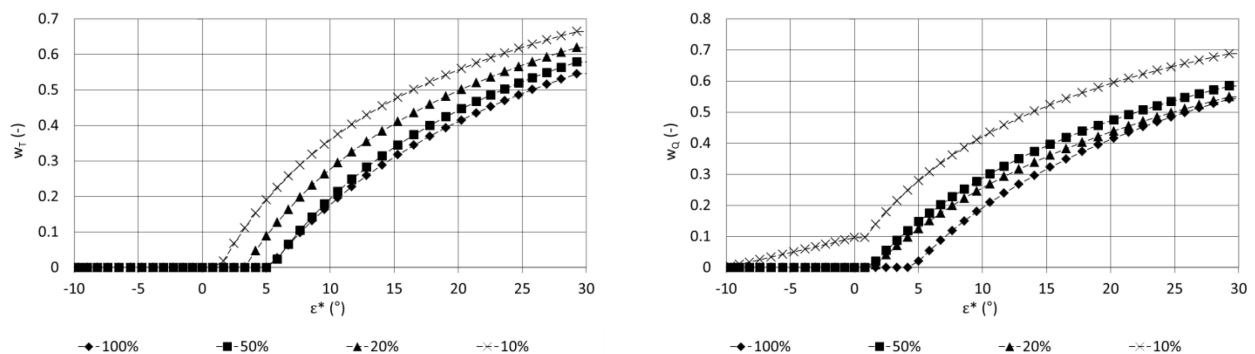
$$v = Y_v \cos 5^\circ = 0.996Y_v \approx Y_v \quad (50)$$

The ship bound axis system can thus still be considered horizontal bound.

3.2 Model of propeller and rudder forces

In the first place the propeller's thrust, the propeller shaft torque and the forces on the rudder have been computed, resulting in the wake factors of Figure 21 and Figure 22.

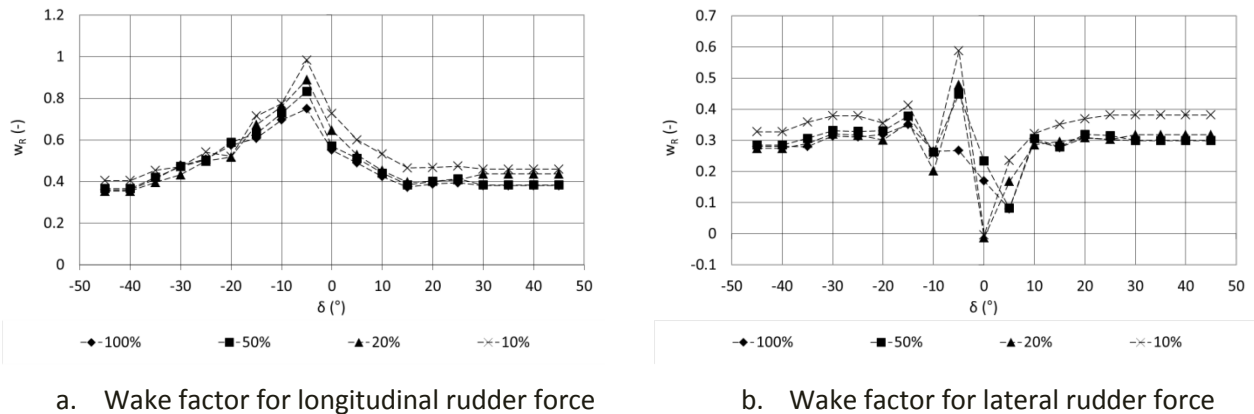
Figure 21 – Wake factors for the propeller thrust and shaft torque



a. Wake factor for propeller thrust

b. Wake factor for propeller shaft torque

Figure 22 – Wake factors for the rudder forces (no drift nor yaw)



The neutral rudder angle is around 5° for all under keel clearances. The thrust, shaft torque and rudder forces are not significantly affected by the heel motion, because the differences between model and measurements are not larger when the roll motion is included compared to the tests without roll motion. In other words, the same mathematical models can be used, without inclusion of any roll motion effects. Of course this may be different in case of a twin rudder – twin propeller ship, for instance the ship model G01 of the Q-flex, which will be modelled later.

3.3 Model of hull forces

3.3.1 Roll dependency

3.3.1.1 Overview

It is obvious from Chapter 2 that the roll motion has a more or less significant effect in all degrees of freedom. These effects are not only dependent of the roll motion, but also on the ship's longitudinal speed. Moreover higher order effects can be observed at higher frequencies and the ship is even prone to parametric rolling, which also exerts significant forces in the horizontal degrees of freedom, but which is out of scope here. To take account of higher order effects in the damping, it was decided to introduce a hydrodynamic angle κ , which expresses the roll speed dependency analogously as the speed components in the other degrees of freedom:

$$\tan \kappa = \frac{0.5pL_{PP}}{u} \quad (51)$$

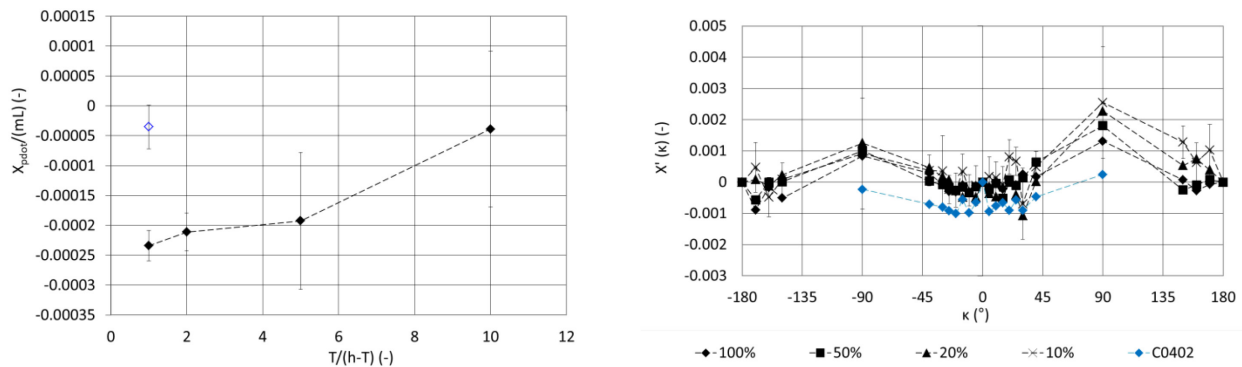
The use of the ship length in the numerator may seem strange in combination with a roll motion, but it allows to have a better spread of κ and a better prediction of the regression results. The effect of κ will be expressed by tabular functions for the different degrees of freedom. The models are expressed for the following κ -values: $0^\circ, \pm 5^\circ, \pm 10^\circ, \dots, \pm 30^\circ, \pm 40^\circ, \pm 90^\circ, \pm 150^\circ, \pm 160^\circ \pm 170^\circ \pm 180^\circ$. The roll dependency models have not only been computed for the loading condition C0401, but also for the loading condition C0402 (blue data points on the figures).

3.3.1.2 Longitudinal force

The roll dependency on the longitudinal force is minor, but yet a mathematical model has been built. The regression coefficients are computed with the program Xphi.f90. For all degrees of freedom the input tests are all harmonic roll tests, and here the following function is evaluated:

$$X = X'_p mL|\dot{p}| + \frac{\rho}{2} LT \left[u^2 + \left(\frac{pL_{PP}}{2} \right)^2 \right] X'(\kappa) + \frac{\rho}{2} LT[u^2] X'(\beta=0) \quad (52)$$

Figure 23 – Roll dependency model for the longitudinal force



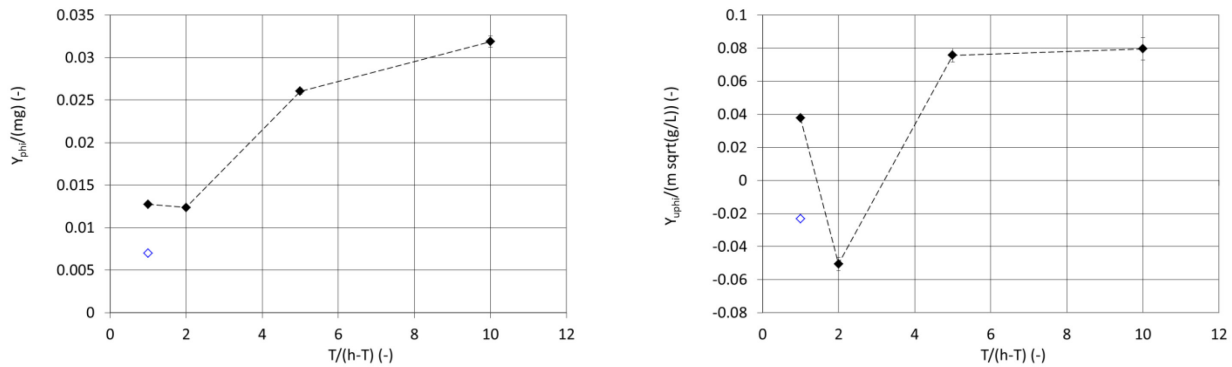
The coefficients have been represented in Figure 23 and the marginal influence of the roll motion is reflected in the significance of the coefficients.

3.3.1.3 Lateral force

The lateral force is computed with the program Yphi.f90, as follows:

$$Y = (Y'_p mL + mz_G) \dot{p} + \frac{\rho}{2} LT \left[u^2 + \left(\frac{pL_{PP}}{2} \right)^2 \right] Y'(\kappa) + \left[Y'_\varphi g + Y'_{u\varphi} u \sqrt{\frac{g}{L}} \right] m\varphi \quad (53)$$

Figure 24 – Roll angle dependent terms for the lateral force



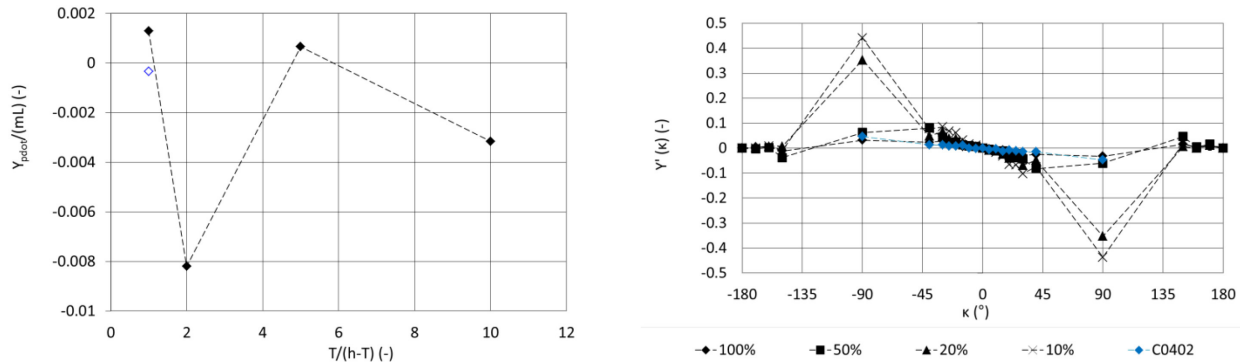
Attention is drawn towards the roll angle dependent terms. As mentioned in Chapter 2 the lateral force is affected by the roll moment which is expressed by Y_φ , on the other hand there is a clear effect of the combination roll angle and longitudinal speed, which has been reported in literature and is modelled with $Y_{u\varphi}$. Both terms are represented in Figure 24:

- Y_φ is more or less constant at the largest under keel clearances and is proportional to \overline{GM} . However its value tends to double for the smaller under keel clearances. This has several reasons. On one hand the maximal roll angle decreases from 5° to 2.5° , but on the other hand the roll moment itself does not decrease due to the increased roll damping (K_p) at smaller under keel clearances. Y_φ is directly connected to the roll moment measurement and should not be included in the simulator. *An open issue is to what extent a correlation occurs between the sway force and the roll moment during the execution of captive model tests.* In case of a dynamic roll motion (variable roll angle), the centre of gravity will oscillate laterally, and this will cause an oscillatory inertia force, which will be measured in the sway force.

- $Y_{u\dot{\varphi}}$ has not only a different sign for the two loading conditions, but also between 50% ukc and the other water depths. The sign swap at 50% ukc is probably a mathematical issue, see also the trend for $Y_{\dot{p}}$ in Figure 25: as both $Y_{u\dot{\varphi}}$ and $Y_{\dot{p}}$ have the wrong sign they may lead to the same result.

The roll velocity dependency has been plotted in Figure 25. The function's magnitude increases with decreasing under keel clearance and increasing \overline{GM} .

Figure 25 – Roll velocity and acceleration dependency model for the lateral force

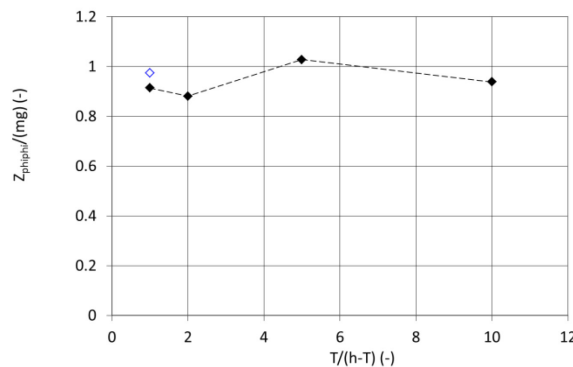


3.3.1.4 Heave force

The roll angle has mainly a hydrostatic effect on the heave force, which is expressed by a quadratic relationship in $Z_{\text{phi.f90}}$:

$$Z = -m y_G \dot{p} - m z_G p^2 + Z'_{\varphi\varphi} m g \varphi^2 + m g T_{rh}^2 Z'(\beta=0) \quad (54)$$

Figure 26 – Roll dependency model for the heave force



The resulting $Z_{\varphi\varphi}$ has been plotted in Figure 26. As expected its value is more or less constant for the different loading conditions and water depths: $Z_{\varphi\varphi} = 0.95 \pm 0.06 \text{ mg}$. At lower ukc frequency effects have been observed, however, it was decided not to include them in the model.

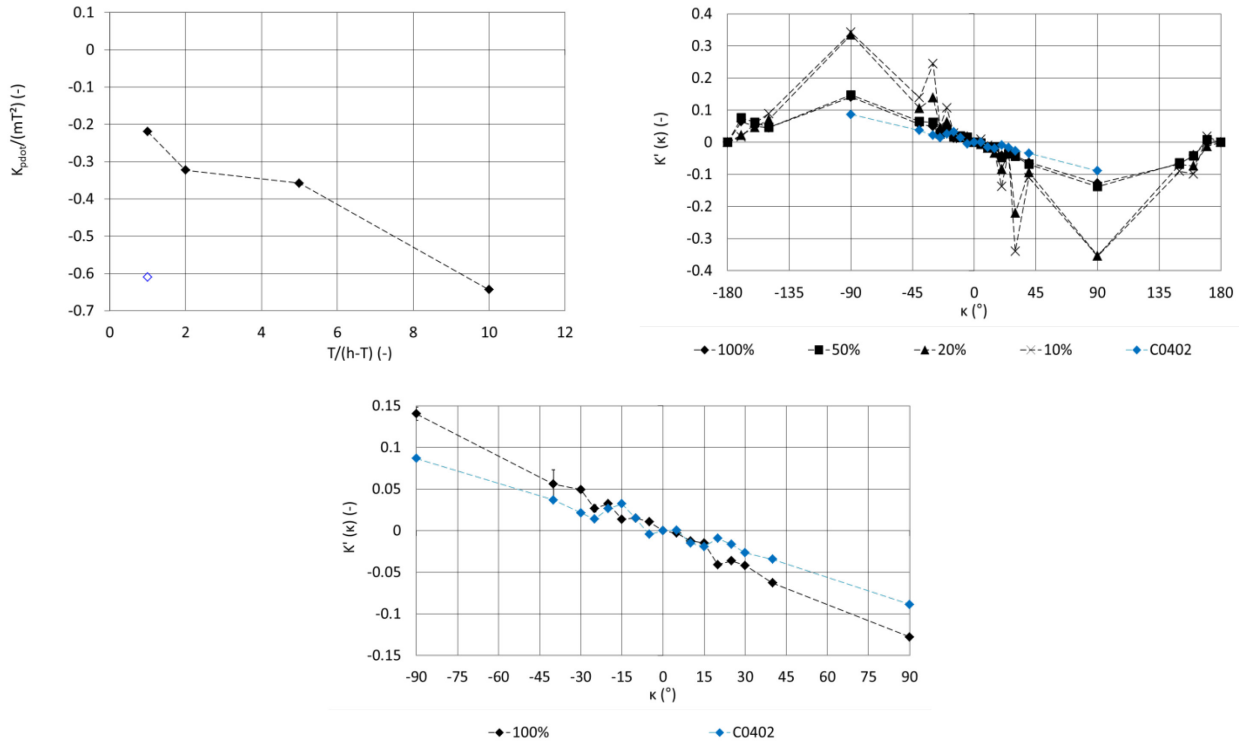
3.3.1.5 Roll moment

In $K_{\text{phi.f90}}$ the regression coefficients of the roll moment are computed:

$$K = \left(K'_{\dot{p}} m T^2 - I_{XX} \right) \dot{p} + \frac{\rho}{2} L T^2 \left[u^2 + \left(\frac{p L_{PP}}{2} \right)^2 \right] K'(\kappa) - m g \overline{GM} \varphi \quad (55)$$

Mind that the roll speed is quadratic, instead of the more common $p|p|$. Regressions were carried out with both options, however no major differences were observed. If $p|p|$ is used, the $K'(\kappa)$ -function becomes symmetric. Figure 27 presents the outcome, based on the quadratic roll speed. K_p increases with decreasing \overline{GM} and under keel clearance. The roll damping function increases with decreasing under keel clearance and increasing \overline{GM} .

Figure 27 – Roll dependency model for the roll moment



3.3.1.6 Pitch moment

As for the heave force the pitch moment is dependent of the roll angle, however, due to the frequency dependency in the roll-pitch coupling a damping function is needed as well, which leads to the following formulation in Mphi.f90:

$$M = M'_{\varphi} mgL\varphi^2 + \frac{\rho}{2} L^2 T \left[u^2 + \left(\frac{pLPP}{2} \right)^2 \right] M'(\kappa) + mgLT_{rh}^2 M'(\beta=0) \quad (56)$$

Figure 28 – Roll dependency model for the pitch moment

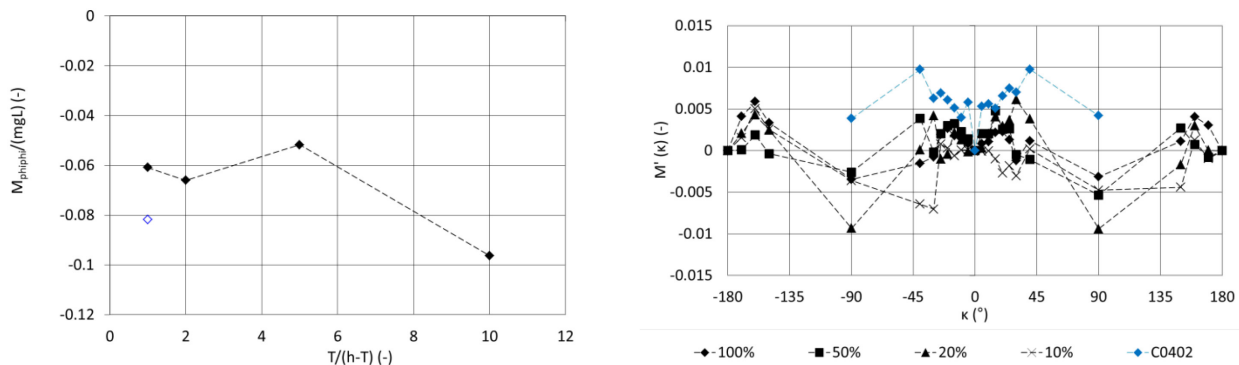


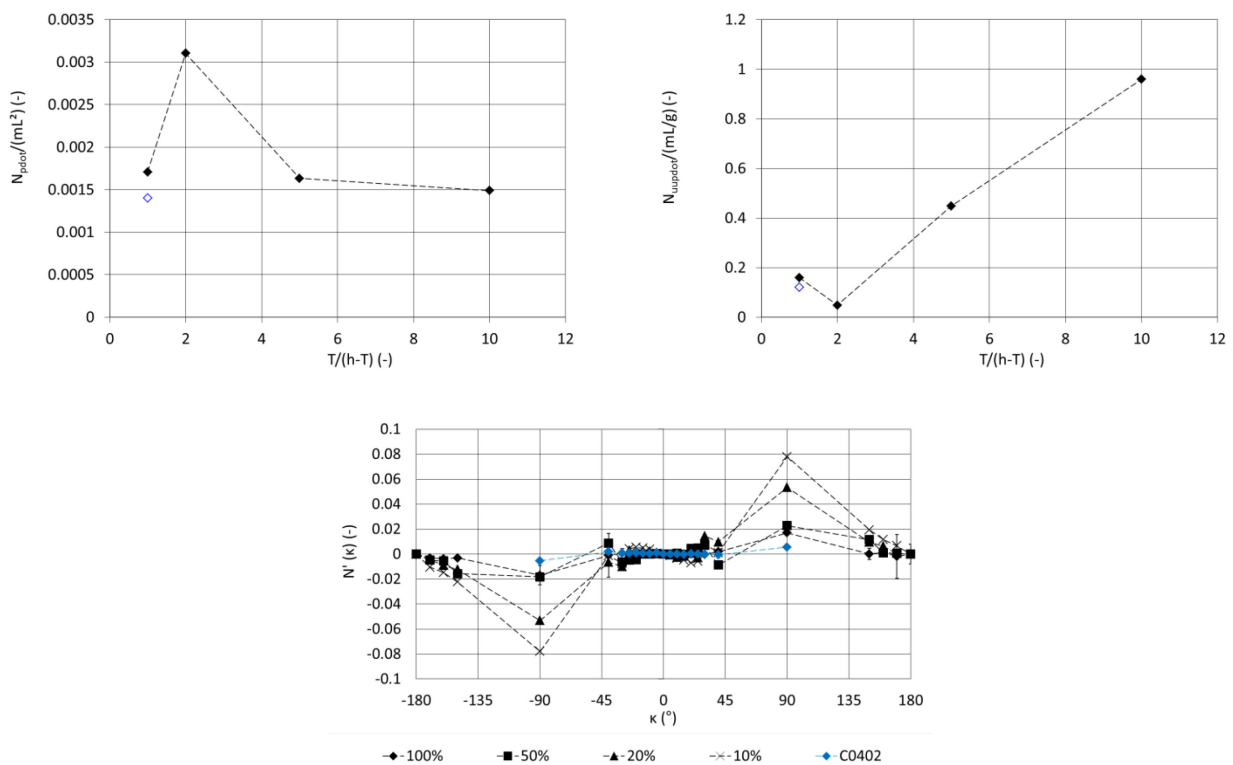
Figure 28 shows the regression coefficients for the different series. Because of the frequency dependency, the supposedly constant hydrostatic term $M_{\varphi\varphi}$ shows more variation compared to the heave force: $M_{\varphi\varphi} = -0.07 \pm 0.02 \text{ mgL}$.

3.3.1.7 Yaw moment

The yaw moment is significantly influenced by the frequency of the roll motion and this dependency increases with the vessel's speed, which leads to the following formulation (Nphi.f90):

$$N = \left(N'_p m L^2 + N'_{uu\dot{p}} m \frac{L}{g} u^2 \right) \dot{p} + \frac{\rho}{2} L^2 T \left[u^2 + \left(\frac{pL_{PP}}{2} \right)^2 \right] N'(\kappa) \quad (57)$$

Figure 29 – Roll dependency model for the yaw moment

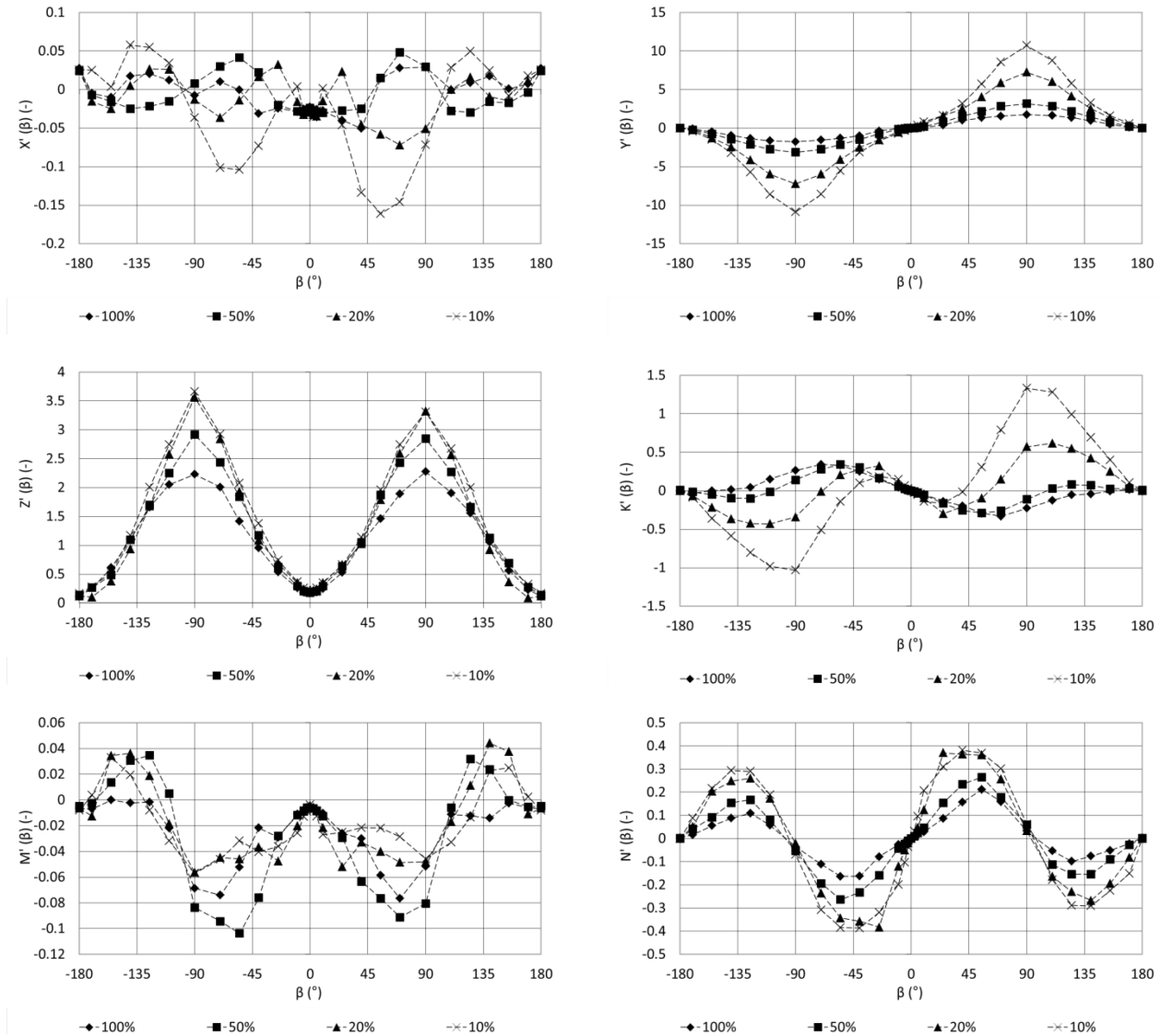


The different coefficients are shown in Figure 29. For 50% ukc there is an unbalance, but for the other conditions $N_{\dot{p}}$ can be considered constant and the speed-frequency dependency increases with decreasing under keel clearance. The same is true for the roll velocity dependency.

3.3.2 Other dependencies

The other components of the hull forces have been modelled like for any other ship model. Figure 30 shows an example for the drift functions which show the known behaviour as a function of the ukc.

Figure 30 – Drift functions for the loading condition C0401



The question then was whether or not roll-sway or roll-yaw coupling should be modelled or not. To do so, the model deviations were investigated as a function of roll angle for tests with yaw or drift. In most of the cases the roll angle had not a significant influence on the deviations, however at small ukc, the sway velocity has an influence on the roll dependency for the sway force and the roll moment, especially if the sway velocity and roll angle have the same sign. As already mentioned in project 13_066 these observations are a result of a complex flow, which can be ascribed to the changed, local under keel clearance of the ship's side that is under attack. It was decided not to include these effects and further adaptation of the mathematical models was not needed.

3.4 Model of propulsion and steering induced forces

As for the propulsion and steering forces, the induced forces and moments have been computed the usual way, i.e. neglecting any possible effects of the roll motion. Some examples for the first quadrant have been shown in Figure 31 and Figure 32.

Figure 31 – Propulsion dependency in the 1st quadrant

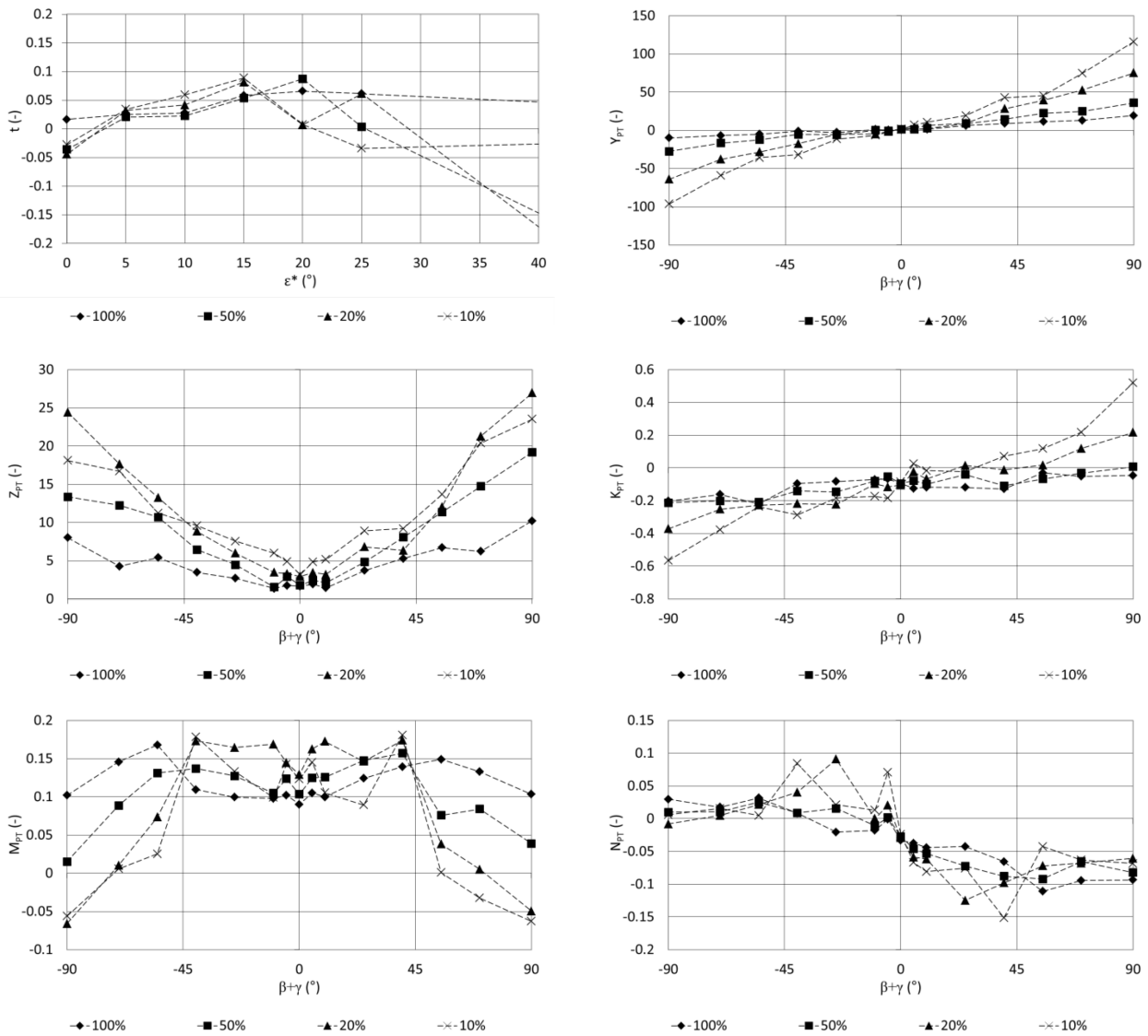
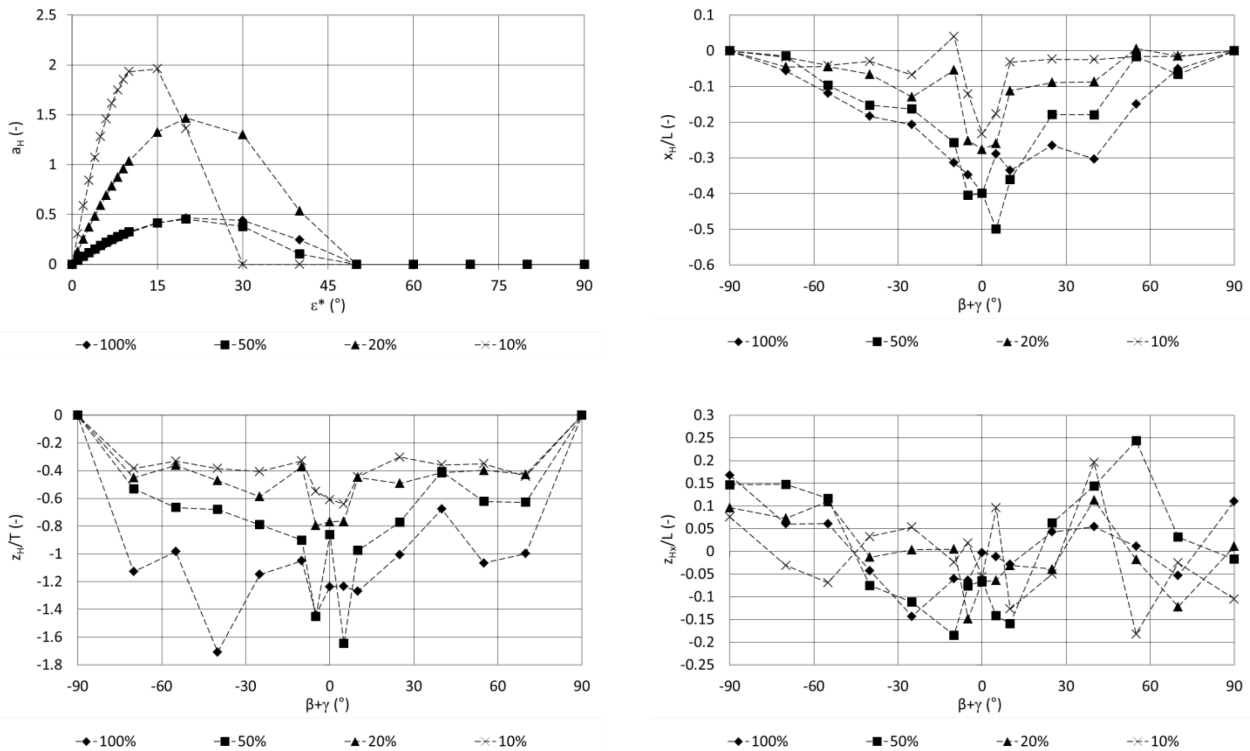


Figure 32 – Rudder dependency in the 1st quadrant



The propulsion and rudder induced forces and moments are neither significantly affected by the heel motion, because the differences between model and measurements are not larger when the roll motion is included compared to the tests without roll motion.

3.5 Validation

Validation is performed in Table 10 by comparing the measured (x) forces and moments with the modelled (y) forces and moment. In general the agreement is acceptable and even excellent for the heave at 100% ukc. The pitch moment is hard to model due to the pitch-roll coupling and the transom section of the KCS.

Table 10 – Comparison between measurements and mathematical model

Series	X	Y	Z	K	M	N
C0401A01	$y = 1.0131x$ $R^2 = 0.956$	$y = 0.9529x$ $R^2 = 0.9557$	$y = 0.9913x$ $R^2 = 0.9889$	$y = 0.9162x$ $R^2 = 0.9902$	$y = 0.9312x$ $R^2 = 0.8511$	$y = 0.958x$ $R^2 = 0.9617$
C0401A02	$y = 1.0306x$ $R^2 = 0.9623$	$y = 0.9245x$ $R^2 = 0.9377$	$y = 0.9817x$ $R^2 = 0.9846$	$y = 0.9123x$ $R^2 = 0.9886$	$y = 0.9775x$ $R^2 = 0.7781$	$y = 0.924x$ $R^2 = 0.938$
C0401A03	$y = 0.9977x$ $R^2 = 0.9712$	$y = 0.9571x$ $R^2 = 0.975$	$y = 0.9469x$ $R^2 = 0.897$	$y = 0.9434x$ $R^2 = 0.9702$	$y = 0.9277x$ $R^2 = 0.8323$	$y = 0.9531x$ $R^2 = 0.9659$
C0401A04	$y = 0.9886x$ $R^2 = 0.9604$	$y = 0.935x$ $R^2 = 0.9684$	$y = 0.9439x$ $R^2 = 0.9235$	$y = 0.9288x$ $R^2 = 0.9295$	$y = 0.8284x$ $R^2 = 0.7932$	$y = 0.9232x$ $R^2 = 0.9392$

4 FAST TIME SIMULATIONS

4.1 Changes to the source code

4.1.1 Default values of tables and coefficients

The file `xml_bindfuncties.f90` has been adapted to allow for default columns in a table, similarly as the default values for `coeff`. For the latter the functions `xwlccoeff` and `xwlccoeff_default` have been merged. An important impact is that whenever `xwlccoeff` is called, this should be now performed with an interface call. At the same time unused variables have been removed from the routine.

4.1.2 Fast time autopilot

The `autopilot.f90` routine has been upgraded for the following manoeuvres:

4.1.2.1 Zigzag and evasive manoeuvres

A new and compacter algorithm has been implemented for the execution of zigzag tests. A new functionality is that now the user can define the yaw checking angle in the autopilot file⁽⁴⁾, in this way any zigzag test can be executed.

The evasive manoeuvres stop now after the maximal duration mentioned in the autopilot file ("*vaarlengte*").

4.1.2.2 REPLAY and COMPUTE trials

The functionality of the REPLAY and COMPUTE trials has been enhanced as follows:

- REPLAY and COMPUTE commands can be given in 6 DOF, respectively `ua`, `va`, `wa`, `pa`, `qa`, `ra` and `u`, `v`, `w`, `p`, `q`, `r`. This also required changes to `WM_parameters.f90`.
- However, the user can select which degrees of freedom should be controlled or not, by simply adding or removing columns in the autopilot file. This functionality has been programmed in `predict.f90` and `predt.f90` and required the upgrade mentioned in 4.1.1. Figure 33 shows a 4 DOF example for a COMPUTE table. Please observe that there is no difference between a REPLAY table without any acceleration columns and a REPLAY_FREE table.

Figure 33 – Example of a 4 DOF COMPUTE table

```
<table name="ComputeCommands" separator=";" ncol="9" nrow="80">
<col name="tijd" type="real" unit="s" lookup="interpol" />
<col name="u" type="real" unit="m/s" />
<col name="v" type="real" unit="m/s" />
```

⁴ Example: `<coeff name="koerswijziging" unit="-" type="real" value="5" comment="Absolute waarde van de hoek in graden waarbij het roer wordt omgeslagen (standaard gelijk aan de absolute waarde van de roerhoek)"></coeff>`

```

<col name="p" type="real" unit="rad/s" />
<col name="r" type="real" unit="rad/s" />
<col name="n1" type="real" unit="/s" />
<col name="n2" type="real" unit="/s" />
<col name="d1" type="real" unit="rad" />
<col name="d2" type="real" unit="rad" />
<row>0;1;0.05;0;0.00349065850398866;0.00438483879697487;0;5.06145483078356E-05;0</row>
...
</table>

```

4.1.3 Full 4 DOF model

The major upgrade consisted in adapting various routines to take account of the newly developed full 4 DOF model. The new coefficients are written to the coefficient XML files which are interpreted in `nb_binden.f90`. The software detects a full 4 DOF model whenever a kappa table is present in the XML file. New public variables have been added to several routines: `nb_idtype.f90`, `nb_krachten_module.f90` and `tab_coefficienten_module.f90`.

The main computation changes are performed in the hull section, namely in `tab_bereken_rompcmp.f90`, where all new full 4DOF computations are added as new functions. At the same time unused variables have been removed and the entire file has been reordered in a more logical X, Y, Z, K, M, N list. The calls to these new functions are performed in the routine `tab_bereken_rompwerking.f90`. In `tab_bereken_krachten.f90` the new parts of the manoeuvring model are included in the interpolations (water depth, draft, mud layer).

Special attention was needed for the roll moment derivatives of previously developed ships, which have been expressed as:

$$\left[K_p - |\varphi| \sqrt{\Delta \overline{GM}_T} \left((-K_{\dot{p}} + I_{xx}) \right) \right] p + K_{up} u p \quad (58)$$

For these ships $K'(\kappa)$ can be expressed as a function of K_p and K_{up} :

$$K'(\kappa) = \frac{\sin \kappa K_p + \sqrt{\left[u^2 + \left(\frac{pL}{2} \right)^2 \right]} \cos \kappa \sin \kappa K_{up}}{0.25 \rho L^2 T^2 \left[u^2 + \left(\frac{pL}{2} \right)^2 \right]} \quad (59)$$

Based on test simulations, the nonlinear, extra damping term $|\varphi| \sqrt{\Delta \overline{GM}_T} \left((-K_{\dot{p}} + I_{xx}) \right)$ should be included in the new model as well.

The equations of motions have been updated accordingly in the routines `correct.f90` and `solve.f90`.

4.1.4 Tuning of coefficients

The routine `bew_xml_module.f90` has been adapted to enable tuning in all 6 DOF, including the newly developed kappa functions. Additional changes were made in `tab_bereken_rompwerking.f90`, `tab_bereken_propulsie.f90` and `tab_bereken_sturing.f90` to take account of the extended tuning possibilities. An example of a full tuning table is shown in Figure 34.

Figure 34 – Example of a full tuning table

```

<!-- Correcties worden toegepast op de wiskundige modellen.
Een parameter van het wiskundige model wordt als volgt gewijzigd
PARAMnieuw = MIN <= PARAMoud * multiplier + shift <= MAX -->
<coeff name="NPARAM" unit="-" type="integer" value="42" comment="aantal in te
<table name="dcoefficient" separator=";" ncol="6" nrow="42" comment="nrow = NP/
  <col name="nr_parameter" type="integer" unit="-" lookup="exact"/>
  <col name="parameter" type="string" unit="-"/>
  <col name="multiplier" type="real" unit="-" comment="multiplier"/>
  <col name="shift" type="real" unit="-" comment="shift"/>
  <col name="minimum" type="real" unit="-" comment="minimale waarde"/>
  <col name="maximum" type="real" unit="-" comment="maximale waarde"/>
  <row>1; Xbeta ; 1.0 ; 0 ; -0.9E+25 ; 0.9E+25</row>
  <row>2; Xgamma ; 1.0 ; 0 ; -0.9E+25 ; 0.9E+25</row>
  <row>3; Xchi ; 1.0 ; 0 ; -0.9E+25 ; 0.9E+25</row>
  <row>4; Xkappa ; 1.0 ; 0 ; -0.9E+25 ; 0.9E+25</row>
  <row>5; Ybeta ; 1.0 ; 0 ; -0.9E+25 ; 0.9E+25</row>
  <row>6; Ygamma ; 1.0 ; 0 ; -0.9E+25 ; 0.9E+25</row>
  <row>7; Ychi ; 1.0 ; 0 ; -0.9E+25 ; 0.9E+25</row>
  <row>8; Ykappa ; 1.0 ; 0 ; -0.9E+25 ; 0.9E+25</row>
  <row>9; Zbeta ; 1.0 ; 0 ; -0.9E+25 ; 0.9E+25</row>
  <row>10; Zgamma ; 1.0 ; 0 ; -0.9E+25 ; 0.9E+25</row>
  <row>11; Zchi ; 1.0 ; 0 ; -0.9E+25 ; 0.9E+25</row>
  <row>12; Kbeta ; 1.0 ; 0 ; -0.9E+25 ; 0.9E+25</row>
  <row>13; Kgamma ; 1.0 ; 0 ; -0.9E+25 ; 0.9E+25</row>
  <row>14; Kchi ; 1.0 ; 0 ; -0.9E+25 ; 0.9E+25</row>
  <row>15; Kkappa ; 1.0 ; 0 ; -0.9E+25 ; 0.9E+25</row>
  <row>16; Mbeta ; 1.0 ; 0 ; -0.9E+25 ; 0.9E+25</row>
  <row>17; Mgamma ; 1.0 ; 0 ; -0.9E+25 ; 0.9E+25</row>
  <row>18; Mchi ; 1.0 ; 0 ; -0.9E+25 ; 0.9E+25</row>
  <row>19; Mkappa ; 1.0 ; 0 ; -0.9E+25 ; 0.9E+25</row>
  <row>20; Nbeta ; 1.0 ; 0 ; -0.9E+25 ; 0.9E+25</row>
  <row>21; Ngamma ; 1.0 ; 0 ; -0.9E+25 ; 0.9E+25</row>
  <row>22; Nchi ; 1.0 ; 0 ; -0.9E+25 ; 0.9E+25</row>
  <row>23; Nkappa ; 1.0 ; 0 ; -0.9E+25 ; 0.9E+25</row>
  <row>24; wrx ; 1.0 ; 0 ; -0.9E+25 ; 0.9E+25</row>
  <row>25; wry ; 1.0 ; 0 ; -0.9E+25 ; 0.9E+25</row>
  <row>26; Fx ; 1.0 ; 0 ; -0.9E+25 ; 0.9E+25</row>
  <row>27; Fy ; 1.0 ; 0 ; -0.9E+25 ; 0.9E+25</row>
  <row>28; aH ; 1.0 ; 0 ; -0.9E+25 ; 0.9E+25</row>
  <row>29; xH ; 1.0 ; 0 ; -0.9E+25 ; 0.9E+25</row>
  <row>30; zH ; 1.0 ; 0 ; -0.9E+25 ; 0.9E+25</row>
  <row>31; XP ; 1.0 ; 0 ; -0.9E+25 ; 0.9E+25</row>
  <row>32; YP ; 1.0 ; 0 ; -0.9E+25 ; 0.9E+25</row>
  <row>33; ZP ; 1.0 ; 0 ; -0.9E+25 ; 0.9E+25</row>
  <row>34; KP ; 1.0 ; 0 ; -0.9E+25 ; 0.9E+25</row>
  <row>35; MP ; 1.0 ; 0 ; -0.9E+25 ; 0.9E+25</row>
  <row>36; NP ; 1.0 ; 0 ; -0.9E+25 ; 0.9E+25</row>
  <row>37; XR ; 1.0 ; 0 ; -0.9E+25 ; 0.9E+25</row>
  <row>38; YR ; 1.0 ; 0 ; -0.9E+25 ; 0.9E+25</row>
  <row>39; ZR ; 1.0 ; 0 ; -0.9E+25 ; 0.9E+25</row>
  <row>40; KR ; 1.0 ; 0 ; -0.9E+25 ; 0.9E+25</row>
  <row>41; MR ; 1.0 ; 0 ; -0.9E+25 ; 0.9E+25</row>
  <row>42; NR ; 1.0 ; 0 ; -0.9E+25 ; 0.9E+25</row>
</table>

```

4.1.5 Functionality fixes

4.1.5.1 Mud density

In `nb_slibgrens_detectie.f90` the following bug has been fixed: if no mud layer is present, the density of the mud layer (instead of the water density) needs to be assigned to the current (water) density.

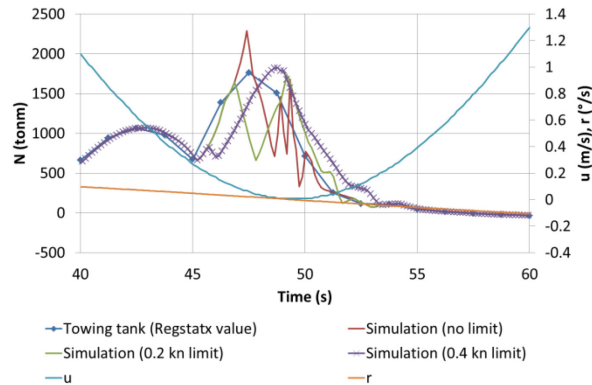
4.1.5.2 Remove unused variables in the propulsion dependent routines

In the routines `tab_bereken_propulsie.f90`, `tab_bereken_propulsiecmp.f90` and `tab_bereken_propulsie_inductie.f90` unused variables have been removed.

4.1.5.3 Selection of yaw angles at very low speed for the rudder induced forces

The `betgam` variable in the function `BepaalVaarhoeken` (routine `tab_bereken_sturingcmp.f90`) is extremely sensitive to oscillations when u is small compared to r . Figure 35 shows an example on the oscillations of the rudder induced yaw moment in such case. The proposed solution is to put a lower limit on the value of u (0.2 or 0.4 kn in Figure 35). The oscillations are less, but the downside is a small phase shift on the model. To enable this limit the function call to `BepaalVaarhoeken` had to be adapted which requires changes to `tab_bereken_sturing.f90` and `tab_bereken_sturing_inductie.f90` as well. At the same time unused variables have been removed.

Figure 35 – COMPUTE simulation of the test C0401A01_MV0300: effect of the limit on the rudder induced yaw moment



4.1.6 Execution of test simulations

The changes described in the previous paragraphs have mainly been performed while executing COMPUTE simulations to compare the simulation outcome with the Regstatx predictions of the towing tank tests. In this way the tabular model has been checked to behave the way it was intended to. To be able to compare with Regstatx predictions, simulations have to be carried out as follows:

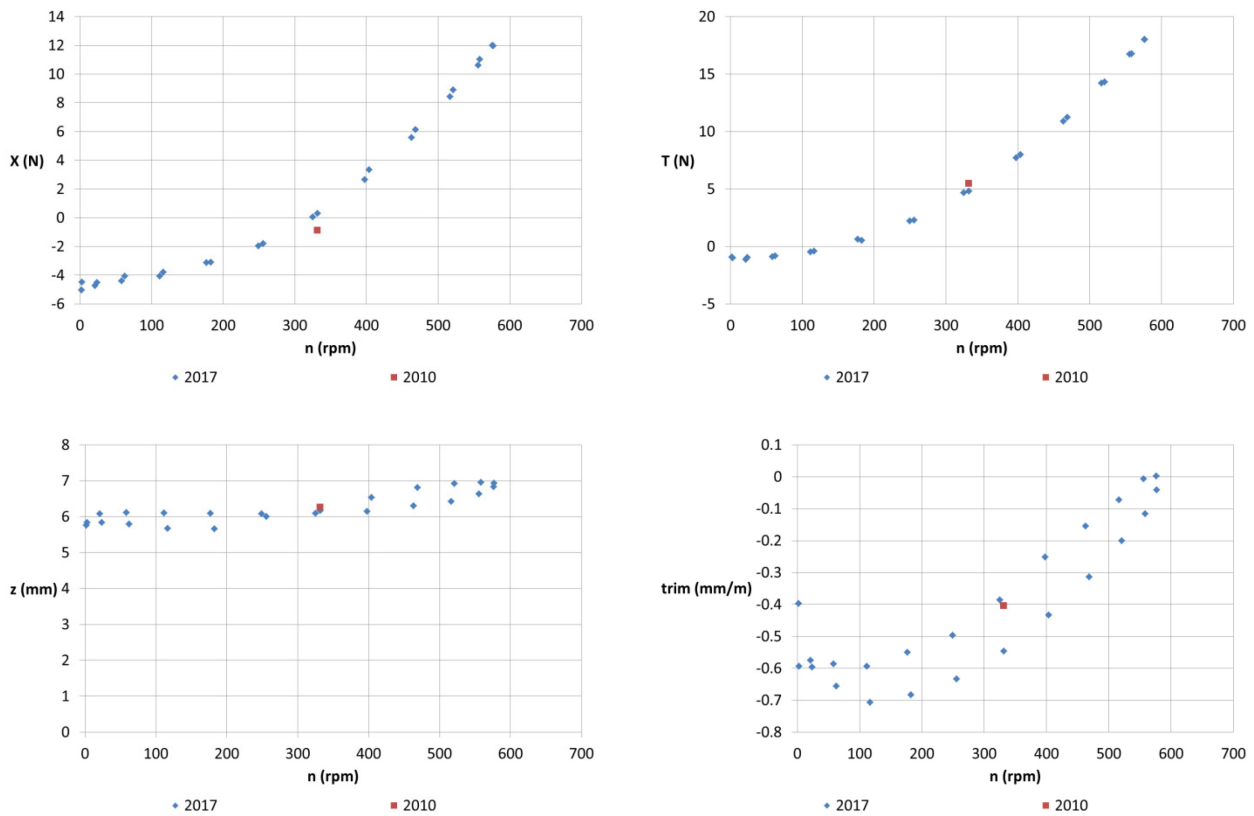
- in fresh water;
- without symmetry corrections;
- without ITTC 1978 correction;
- with the numerically added components equal to zero: $|\varphi| \sqrt{\Delta \overline{GM}_T \left((-K_{\dot{p}} + I_{xx}) \right)}, Z_w, Z_q, M_w, M_q$.

4.2 Comparison with SIMMAN2014 results

4.2.1 Captive tests

In the frame of SIMMAN 2014 both captive and free running model tests have been executed with a 1/52.667 scale model of the KCS built by SVA (code C01). The free running tests can be compared with simulation runs, but prior to this, the captive test results of both ships have been compared. Figure 36 shows an example of the resistance and propulsion behaviour. All tests with C01 (2010) were carried out at the assumed straight line self-propulsion point. However as can be seen in Figure 36 a slightly negative longitudinal force was obtained for C01, while C04 (2017) gives a correct self-propulsion point. Moreover at the same time the measured thrust was slightly higher for C01 compared to C04 (in both conditions the same propeller shaft torque was measured). The agreement for sinkage and trim is acceptable.

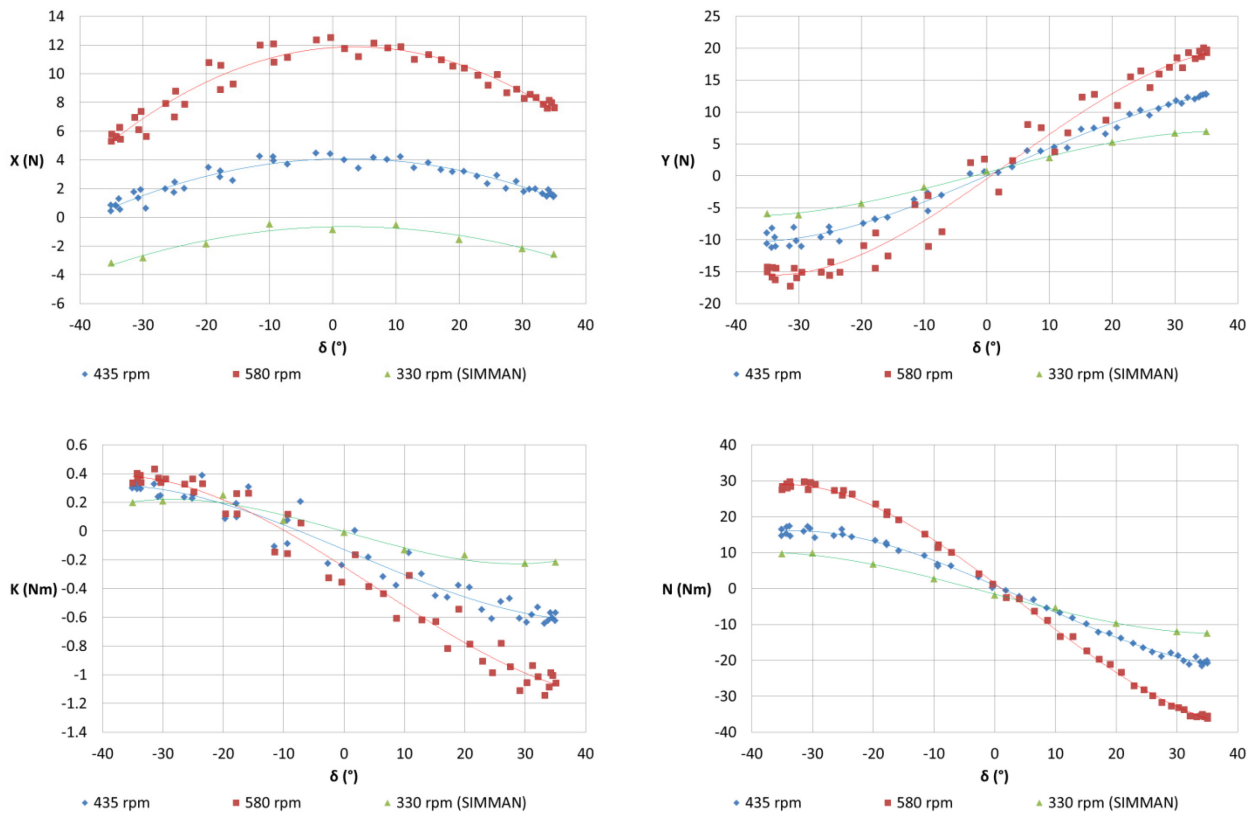
Figure 36 – Comparison of resistance and propulsion tests between 2010 and 2017: 20% ukc, 0.62 m/s



The effect of the rudder variation has been compared in Figure 37. Although there are no tests performed at the same propeller rate, the trends as a function of propeller rate and rudder angle seem acceptable. The attention is drawn to the rudder angle at which the yaw moment turns zero. There seems to be an offset of 5° between the 2010 and 2017 tests. Unluckily there are no rudder force measurements available from the 2010 test.

Based on the above comparison the captive model test results are similar, but there seem to be some differences in self-propulsion point and neutral rudder angle.

Figure 37 – Comparison of rudder tests between 2010 and 2017: 20% ukc, 0.62 m/s

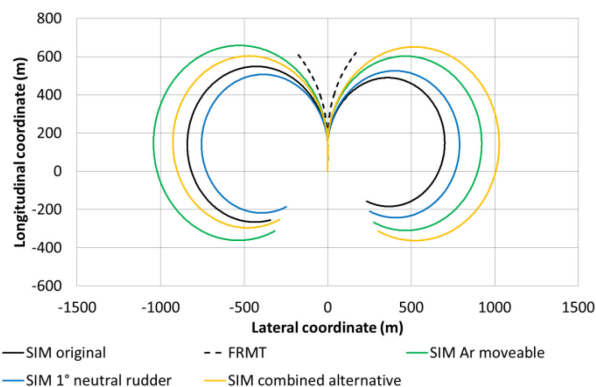


4.2.2 Free running tests

The SIMMAN 2014 free running tests were executed in 2010, but only at 20% ukc. Due to problems with rudder friction, the rudder steering rate was lower than expected: $1^\circ/s$ full scale instead of $2.32^\circ/s$. To perform the comparison the rudder speed for the simulations was set to $1^\circ/s$.

Figure 38 shows the comparison between the simulated turning circles and the free running results. Different alternative simulations were carried out because the original data (SIM original: Regstatx based, but with hull symmetry) showed better initial turning behaviour and larger port-starboard asymmetry:

Figure 38 – Comparison between free running initial turning circles and different simulation alternatives

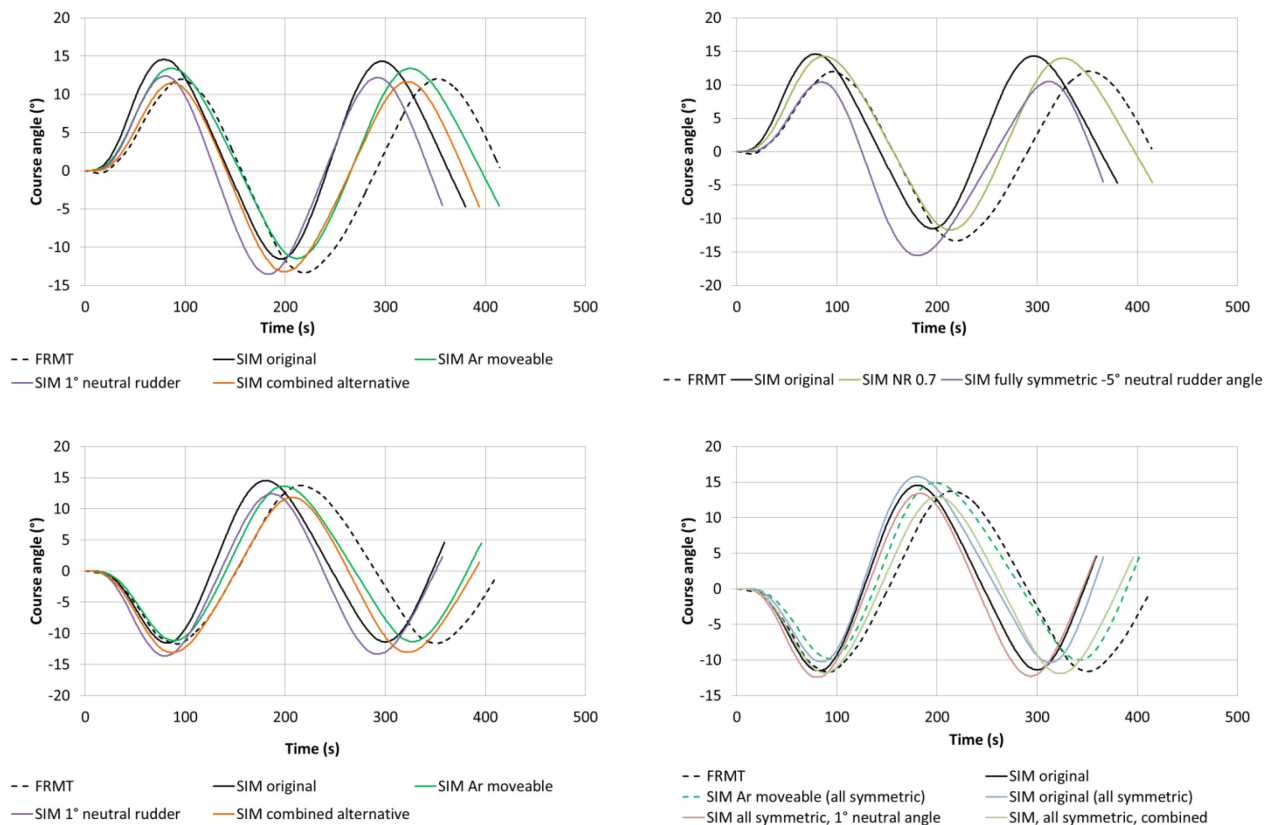


- The alternative simulation with the rudder downgraded to only the movable part (SIM Ar moveable), results in a slower turning, but yet significantly below the free running trials;
- Another alternative lowered the neutral rudder angle to 1° instead of 5°. With this setting the port-starboard unbalance is removed;
- The combination of both (SIM combined alternative) however leads now to a larger starboard circle, but still below the free running trial.

Figure 39 shows the comparison between the free running zigzag tests and simulated zigzag tests:

- The original simulation data show a larger overshoot, a smaller period and a better turning behaviour to starboard side compared to the free running trials;
- Only taking account of the movable area of the rudder decreases the overshoots and increases the zigzag period. For both initial zigzag directions the period is still smaller compared to the free running trials, however the overshoots are better predicted when starting to portside;
- One of the reasons is that the free running trials are quite symmetric, except for the onset to portside when the manoeuvre is performed to starboard. This onset can more or less be controlled by changing the neutral rudder angle to its opposite value, but this leads also to a vertical shift of the manoeuvre (when not only the hull forces, but also the propeller and rudder forces are made symmetric);
- Setting the neutral rudder angle to +1° in the original simulation model predicts the correct overshoot when starting to starboard, but causes a vertical shift when starting to portside;
- The combination of neutral rudder angle at +1° and movable area is the closest fit when starting to starboard (apart from the period), but causes again a vertical shift when starting to portside. For the latter the best fit is using the same alternative but with a simulation model that has hull, propeller and rudder symmetry.

Figure 39 – Comparison between free running zigzag tests and different simulation alternatives



It can be observed from the above that the neutral rudder angle can significantly affect the output from the simulation. In the meantime the same technique was applied to solve asymmetries with the Triple E. Moreover it seems that this neutral rudder angle is different for the two KCS variants. Due to the fact that there have been problems with the rudder for the SIMMAN KCS, it has been decided not to tune the mathematical model based on the comparison with the SIMMAN free running tests yet. Ideally new free running tests with the ship model C04 should be executed. The agreement with the present free running data is worse compared to the KVLCC2 without tuning [5].

4.3 Standard manoeuvres: first iteration

All standard manoeuvres are carried out with the original simulation model (hull forces were made symmetric). Acceleration trials were carried out at the telegraphs positions mentioned in Table 11. The obtained speeds are mentioned in Figure 40. Mind that speeds above the red line are not realistic, because the ship sinks more than the available under keel clearance. The maximal telegraph setting which is acceptable for all under keel clearances is Slow. The turning circles and zigzag tests are therefore carried out at this setting.

Table 11 – Telegraph positions for the simulations

Position ahead	rpm	Position astern	rpm
Full	71	Full	-71
Half	58	Half	-58
Slow	41	Slow	-41
Dead slow	30	Dead slow	-30

Figure 40 – Obtained speeds (red curve indicates sinkage limit)

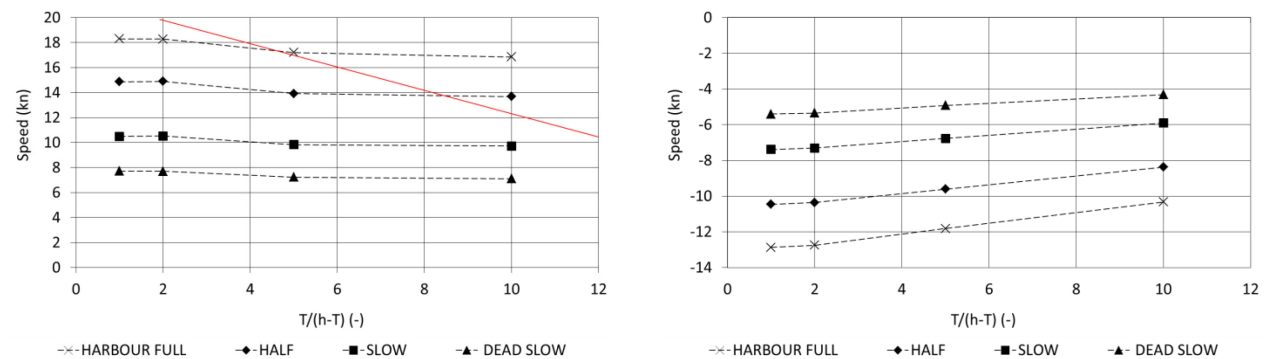
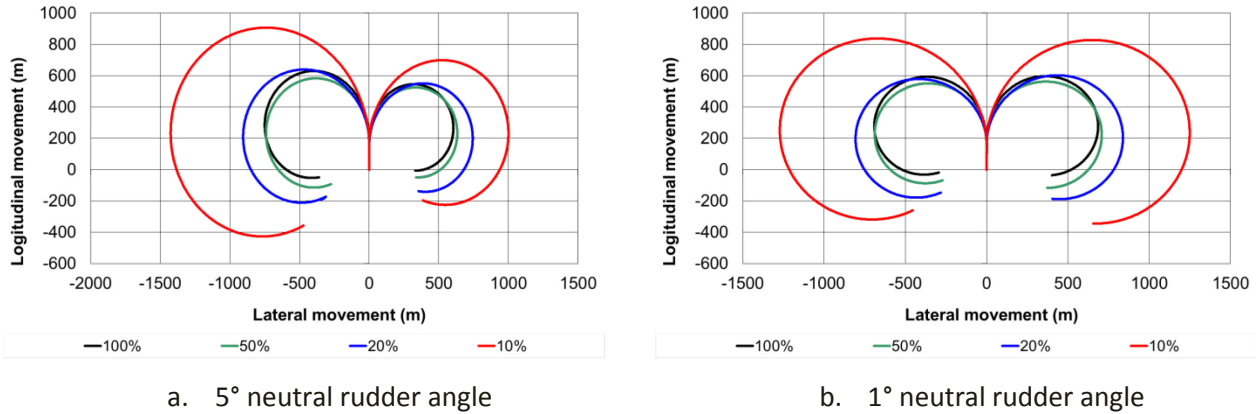


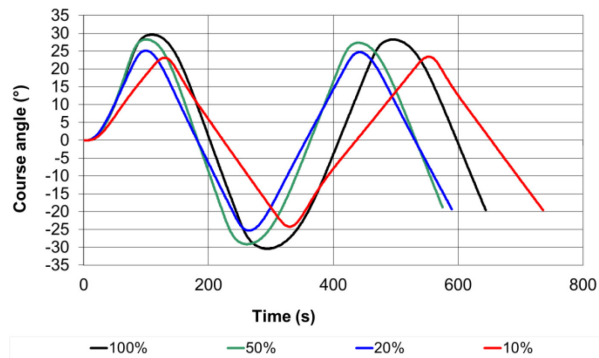
Figure 41a shows the resulting trajectories with the original neutral rudder angles. A significant asymmetry is observed between the turning circles to starboard and to port. Also the initial turning behaviour at 100% ukc is not satisfactory. The portside-starboard side asymmetry can be decreased by lowering the neutral rudder angle from 5° to 1°. The resulting trajectories have been plotted in Figure 41b.

Figure 41 – First iteration turning circles



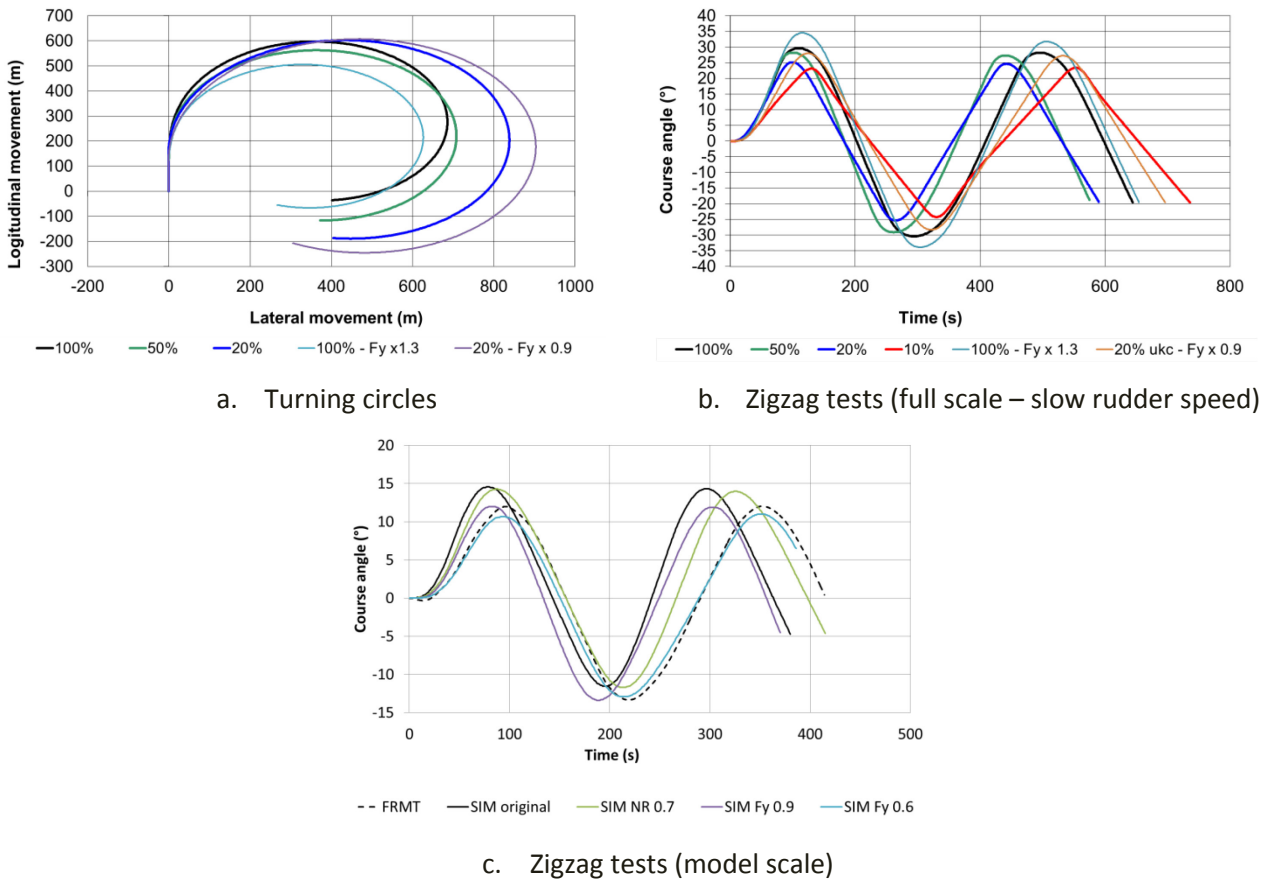
The zigzag test shown in Figure 42 have been carried out with 1° neutral rudder angle. The zigzag seems to sluggish at 100% ukc and too quick at 20% ukc, which is also the under keel clearance of the free running tests.

Figure 42 – First iteration zigzag trials



Summarised, the turning behaviour should be enhanced at 100% ukc and weakened at 20% ukc. Based on the evolution of the force components during the manoeuvre it was decided to tune the lateral rudder force. A better evolution as a function of the under keel clearance is obtained when the lateral rudder force is multiplied with 1.3 at 100% ukc and with 0.9 at 20% ukc (see Figure 43), however the lateral rudder force should be decreased more drastically to have a better match with the free running manoeuvre at 20% ukc (0.6 instead of 0.9). This may not only be due to scale effects, but also due to the different nature of the zigzag manoeuvres (20/20 vs 20/5).

Figure 43 – Tuned manoeuvres



4.4 Standard manoeuvres: second iteration

4.4.1 Acceleration trials

Figure 44 shows the obtained speeds after tuning. Again some ahead speeds are not achievable due to excessive sinkage. All other manoeuvres will therefore focus on the telegraph position Slow.

Figure 44 – Obtained speeds

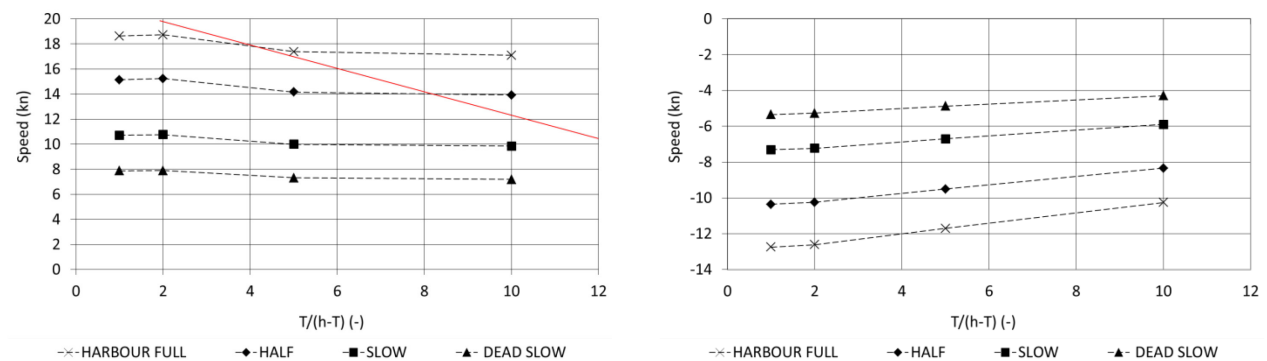
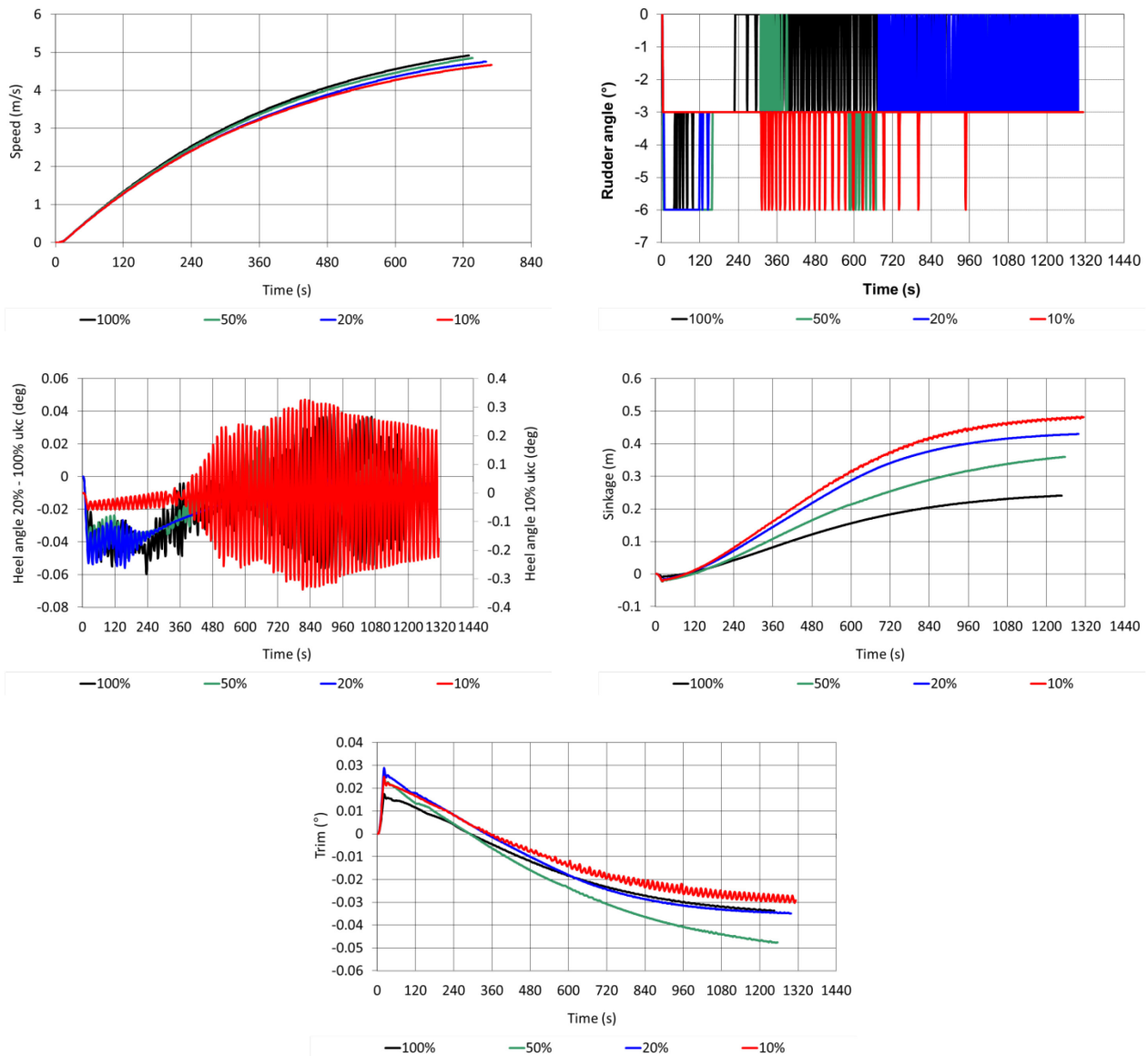


Figure 45 – Selection of time series while acceleration at telegraph position Slow

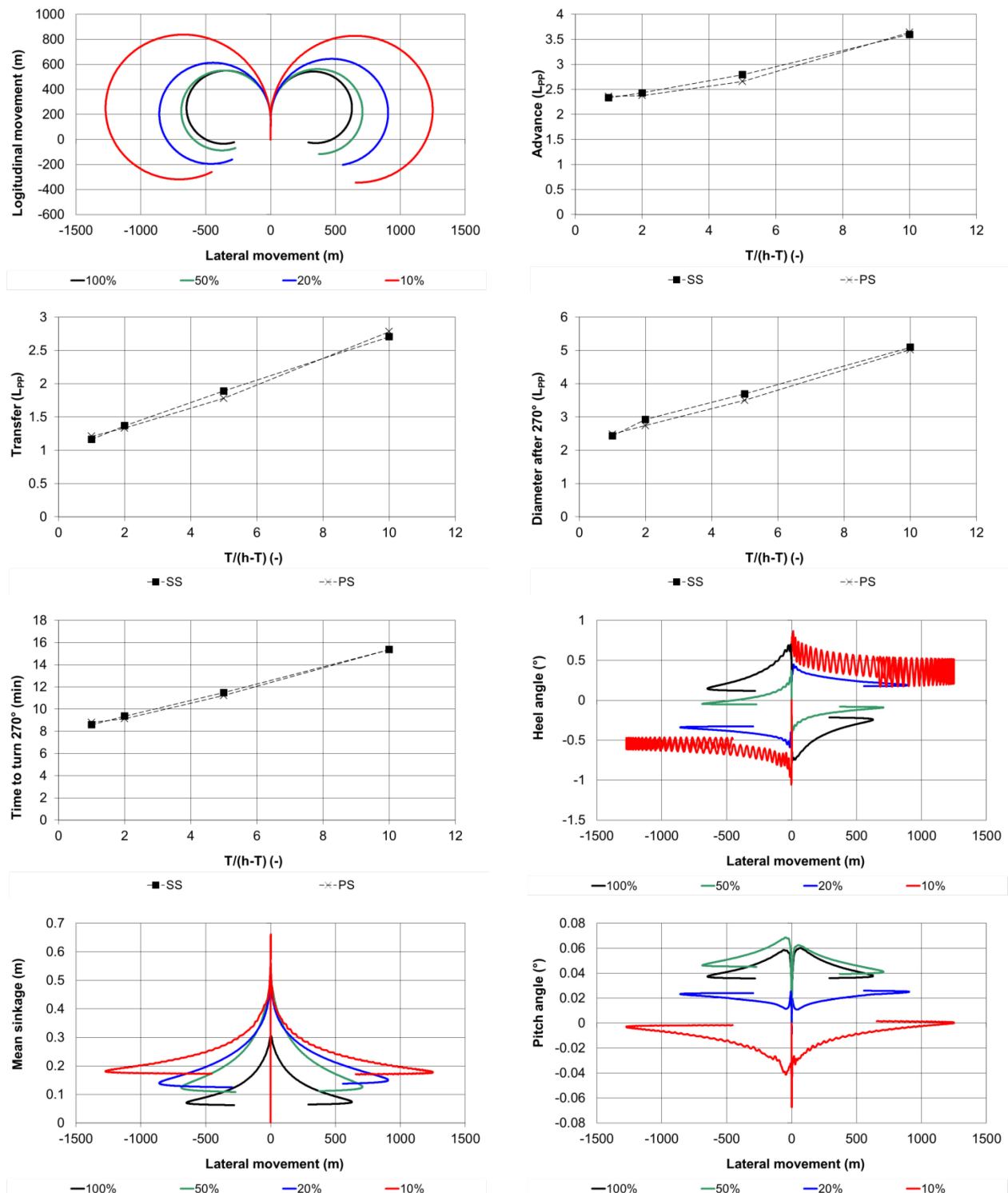


In Figure 45 the most relevant time signals have been shown. The rudder angle is mostly set at a small negative value to maintain a straight track. This negative value is caused by the shift of the neutral rudder angle from 5° to 1°. Rudder actions have a direct influence on the heel angle, which is the largest (+/- 0.3°) at the smallest under keel clearance.

4.4.2 Turning circles

Figure 46 shows the main parameters of the 35° turning circles at telegraph position Slow. The evolution as a function of the under keel clearance is better due to the tuning of the lateral force, while the asymmetry has been decreased due to the neutral rudder angle. The outward heel at larger under keel clearances changes into inward heel at 10 and 20% ukc, but during the free running test the heel is still outward at 20% ukc. The damping of the heel motion seems difficult at 10% ukc. Due to the speed reduction while turning the sinkage reduces significantly.

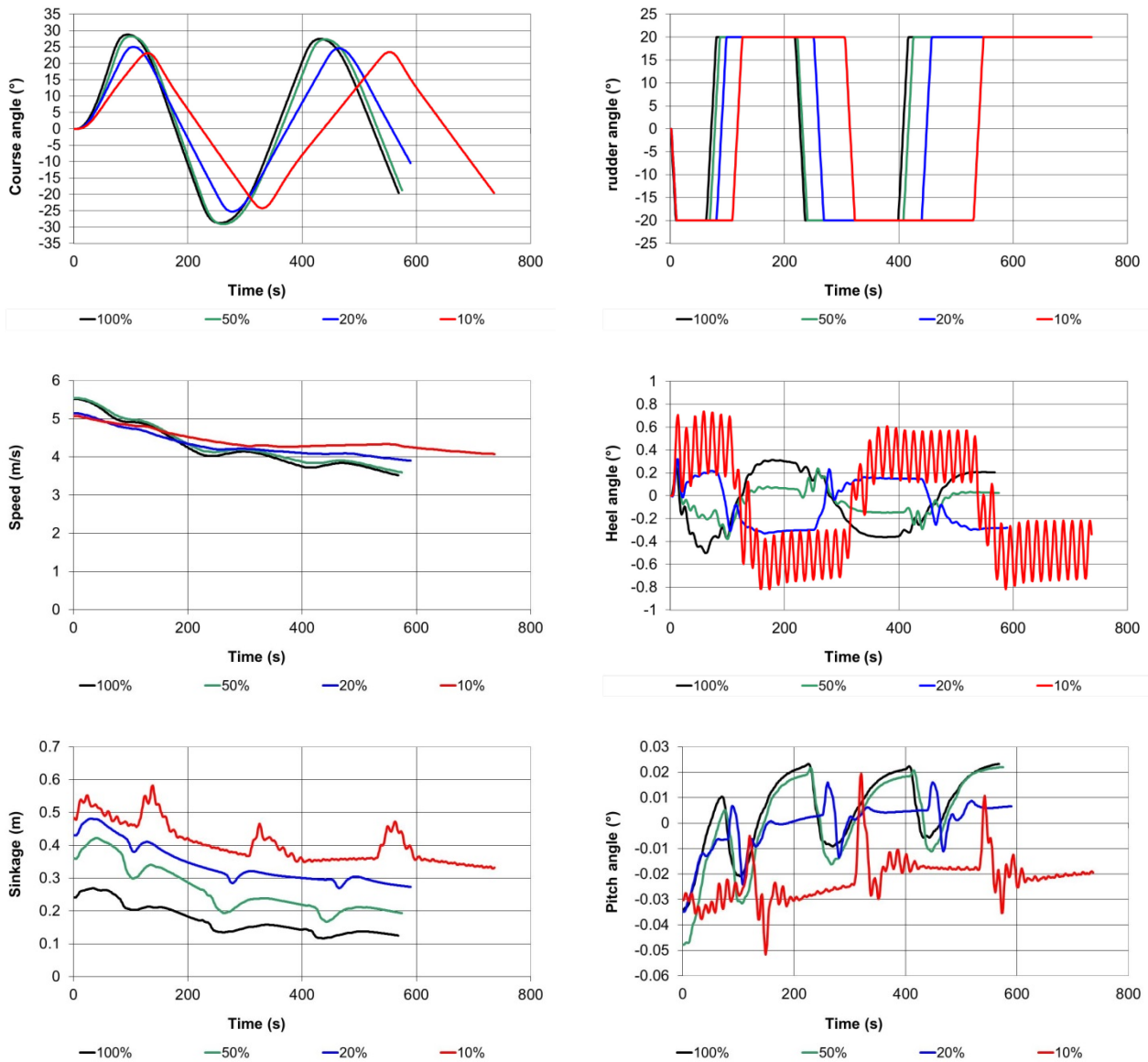
Figure 46 – 35° turning circles at telegraph position Slow



4.4.3 Zigzag tests

Figure 47 shows the relevant parameters of the 20/20 zigzag tests at telegraph position Slow. Due to the tuning the overshoot angles decrease and the period increases with decreasing under keel clearance. The speed drop during the manoeuvre is more significant at larger under keel clearances. Again the heel motion is opposite and less damped at smaller under keel clearances.

Figure 47 – 20/20 zigzag tests at telegraph position Slow



4.4.4 Crash stop tests

To perform the crash stop tests the KCS was fitted with the same engine as the Asya_5000TEU, but the B-coefficients were decreased due to the smaller propeller size and to achieve a less powerful engine. Of course the results here are highly affected by the engine performance. Figure 48 gives an idea of the implemented performance.

Figure 48 – Crash stop test performance: evolution of propeller rate

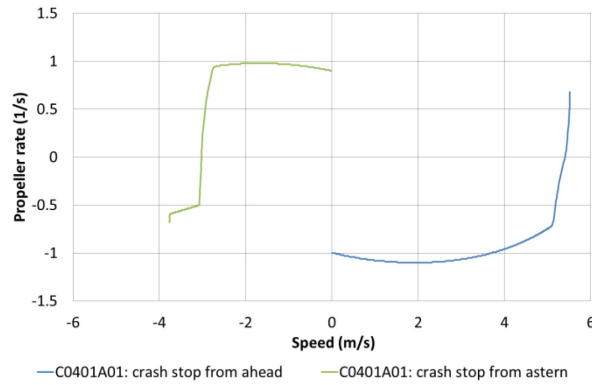
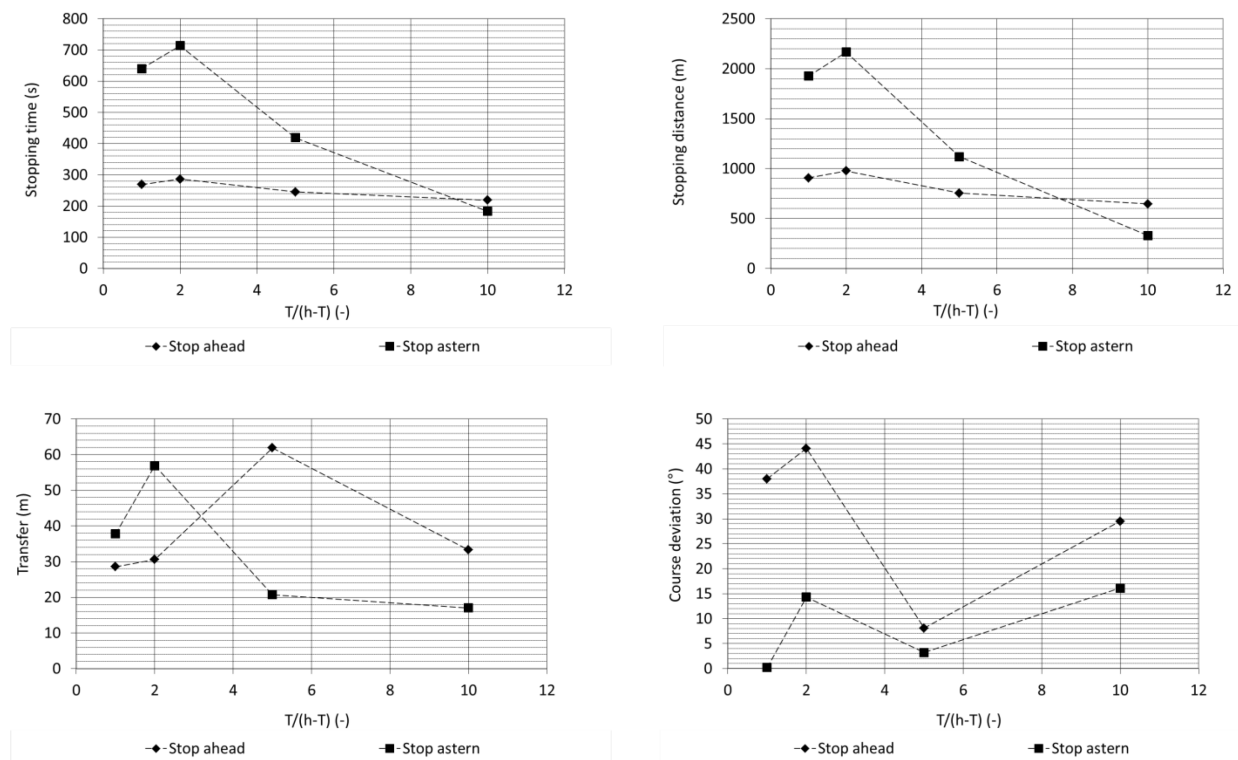


Figure 49 – Crash stop tests starting from telegraph position Slow



The results from the crash stops are represented in Figure 49. In most cases the ship is able to stop within reasonable limits, however transfer and especially course deviations can be significant at larger under keel clearances.

5 CONCLUSIONS AND RECOMMENDATIONS

5.1 Conclusions

In this report the open water tests with the benchmark ship KCS have been studied. The newly implemented roll engine on the towing carriage was used to conduct an extensive study on the rolling behaviour of the ship. The KCS seems particularly vulnerable to roll due to its transom's shape. This vulnerability was also shown with the execution of parametric roll tests.

The mathematical manoeuvring models have been adapted to cope with the additional captive roll motion and resulting measurements. The simulator was adapted accordingly and received additional upgrades. Fast time simulations showed once again that tuning of the model was necessary in order to achieve realistic manoeuvres.

5.2 Recommendations

- SIMMAN 2014 indicated that the manoeuvring behaviour of the KCS required the roll to be included for good predictive capabilities. It seemed however difficult to separate the effect of the roll from the other degrees of freedom in the simulator code. More flexibility is required to turn degrees of freedom on or off.
- The test program in the towing tank should be adapted to the needs of the ship manoeuvring simulator. Therefore a study of the coverage of kinematic and control parameters during real time simulation runs is required.
- Outliers in the tabular models can have a negative effect on the simulations. Tools should be automated to detect these outliers. More in general, the current tabular model which has been developed for the last 15 years should be checked for robustness and a better balance is needed between the different components of the modular model (e.g. the wake of the thrust is expressed as a function of the propeller loading, while the wake of the rudder is expressed as a function of rudder angle) to create a tabular model 2.0.
- A more comprehensive study with multiple \overline{GM}_T and draft variations is needed to fully capture the effect on the roll moment.
- An open issue to be investigated is to what extent a correlation occurs between the sway force and the roll moment during the execution of captive model tests.

6 REFERENCES

- [1] <https://simman2014.dk/ship-data/moeri-container-ship/geometry-and-conditions-moeri-container-ship/>
- [2] <http://wlsow.vlaanderen.be/shpgenerator/default.aspx>
- [3] **Delefortrie, G.; Eloot, K.; Peeters, P.; Mostaert, F.** (2016). Modelling the Manoeuvring Behaviour of Maersk Triple E: Sub report 3 : Model and Simulations for 12 m Draft, including Heeled Loading. Version 3.0. WL Reports, 13_066. Flanders Hydraulics Research: Antwerp, Belgium.
- [4] **American Bureau of Shipping** (2008). Guide for the assessment of parametric roll resonance in the design of container carriers. Houston, USA.
- [5] **Delefortrie, G.; Eloot, K.; Lataire, E.; Van Hoydonck, W.; Vantorre, M.** (2016). Captive Model Tests Based 6 DOF Shallow Water Manoeuvring Model, MASHCON 2016, Hamburg, Germany.

DEPARTMENT **MOBILITY & PUBLIC WORKS**
Flanders hydraulics Research

Berchemlei 115, 2140 Antwerp

T +32 (0)3 224 60 35

F +32 (0)3 224 60 36

waterbouwkundiglabo@vlaanderen.be

www.flandershydraulicsresearch.be